

*ARMY RESEARCH LABORATORY*



# **The Effects of Layer Constraint on Stress Wave Propagation in Multilayer Composite Materials**

**by Alper Tasdemirci, Ian W. Hall, Bazle A. Gama, and Mustafa Guden**

**ARL-CR-550**

**September 2004**

**prepared by**

**Department of Mechanical Engineering  
University of Delaware  
Center for Composite Materials  
Newark, DE 19716**

**under contract**

**DAAD19-01-2-0001**

## **NOTICES**

### **Disclaimers**

The findings in this report are not to be construed as an official Department of the Army position unless so designated by other authorized documents.

Citation of manufacturer's or trade names does not constitute an official endorsement or approval of the use thereof.

Destroy this report when it is no longer needed. Do not return it to the originator.

# **Army Research Laboratory**

Aberdeen Proving Ground, MD 21005-5069

---

---

**ARL-CR-550**

**September 2004**

---

---

## **The Effects of Layer Constraint on Stress Wave Propagation in Multilayer Composite Materials**

**Alper Tasdemirci, Ian W. Hall, and Bazle A. Gama**  
**Department of Mechanical Engineering and**  
**Center for Composite Materials**  
**University of Delaware**

**Mustafa Guden**  
**Department of Mechanical Engineering,**  
**Izmir Institute of Technology**

**prepared by**

**Department of Mechanical Engineering**  
**University of Delaware**  
**Center for Composite Materials**  
**Newark, DE 19716**

**under contract**

**DAAD19-01-2-0001**

Report Documentation Page			Form Approved OMB No. 0704-0188		
Public reporting burden for this collection of information is estimated to average 1 hour per response, including the time for reviewing instructions, searching existing data sources, gathering and maintaining the data needed, and completing and reviewing the collection information. Send comments regarding this burden estimate or any other aspect of this collection of information, including suggestions for reducing the burden, to Department of Defense, Washington Headquarters Services, Directorate for Information Operations and Reports (0704-0188), 1215 Jefferson Davis Highway, Suite 1204, Arlington, VA 22202-4302. Respondents should be aware that notwithstanding any other provision of law, no person shall be subject to any penalty for failing to comply with a collection of information if it does not display a currently valid OMB control number. <b>PLEASE DO NOT RETURN YOUR FORM TO THE ABOVE ADDRESS.</b>					
1. REPORT DATE (DD-MM-YYYY) September 2004		2. REPORT TYPE Final		3. DATES COVERED (From - To) September 2003	
4. TITLE AND SUBTITLE The Effects of Layer Constraint on Stress Wave Propagation in Multilayer Composite Materials			5a. CONTRACT NUMBER DAAD19-01-2-0001		
			5b. GRANT NUMBER		
			5c. PROGRAM ELEMENT NUMBER		
6. AUTHOR(S) Alper Tasdemirci,* Ian W. Hall,* Bazle A. Gama,* and Mustafa Guden <sup>†</sup>			5d. PROJECT NUMBER 622618.AH80		
			5e. TASK NUMBER		
			5f. WORK UNIT NUMBER		
7. PERFORMING ORGANIZATION NAME(S) AND ADDRESS(ES) University of Delaware Department of Mechanical Engineering Center for Composite Materials Newark, DE 19716			8. PERFORMING ORGANIZATION REPORT NUMBER		
9. SPONSORING/MONITORING AGENCY NAME(S) AND ADDRESS(ES) U.S. Army Research Laboratory ATTN: AMSRD-ARL-WM-MB Aberdeen Proving Ground, MD 21005-5066			10. SPONSOR/MONITOR'S ACRONYM(S) ARL-CR-550		
			11. SPONSOR/MONITOR'S REPORT NUMBER(S)		
12. DISTRIBUTION/AVAILABILITY STATEMENT Approved for public release; distribution is unlimited.					
13. SUPPLEMENTARY NOTES *Department of Mechanical Engineering and Center for Composite Materials, University of Delaware, Newark, DE 19716 <sup>†</sup> Department of Mechanical Engineering, Izmir Institute of Technology, Izmir, Gulbahce, Turkey					
14. ABSTRACT Multilayer materials consisting of ceramic and glass/epoxy with a rubber interlayer have been subjected to a high strain rate compression using a split-Hopkinson Pressure Bar (SHPB). The feasibility of modeling stress wave propagation in complex multilayer materials has been demonstrated. It has been shown that the effects of lateral confinement of a normally low-modulus interlayer material can significantly affect the response to wave propagation.  Numerical modeling clearly shows that severe stress inhomogeneities and discontinuities exist, and these may have serious consequences for the mechanical and other properties. The one-dimensional stress state usually assumed for conventional SHPB testing is therefore inapplicable, and both numerical and experimental results have to be coupled for a complete understanding of the wave propagation characteristics. In this study, both methods were used, and the stress states inside the components were presented.					
15. SUBJECT TERMS multilayer structures, finite element analysis, mechanical properties, high strain rate					
16. SECURITY CLASSIFICATION OF:			17. LIMITATION OF ABSTRACT  UL	18. NUMBER OF PAGES  44	19a. NAME OF RESPONSIBLE PERSON Alper Tasdemirci
a. REPORT UNCLASSIFIED	b. ABSTRACT UNCLASSIFIED	c. THIS PAGE UNCLASSIFIED			19b. TELEPHONE NUMBER (Include area code) 302-831-8850

---

## Contents

---

<b>List of Figures</b>	<b>iv</b>
<b>List of Tables</b>	<b>iv</b>
<b>Acknowledgments</b>	<b>v</b>
<b>1. Introduction</b>	<b>1</b>
<b>2. Experiments and Modeling</b>	<b>2</b>
<b>3. Results</b>	<b>5</b>
3.1 Impact Velocity (10 m/s).....	5
3.2 Impact Velocity (16 m/s).....	6
3.3 Impact Velocity (20.5 m/s).....	9
<b>4. Discussion</b>	<b>13</b>
<b>5. Conclusions</b>	<b>17</b>
<b>6. References</b>	<b>18</b>
<b>Distribution List</b>	<b>21</b>

---

## List of Figures

---

Figure 1. (a) Constrained sample prior to testing and (b) schematic of setup. ....	3
Figure 2. Stress on the incident and transmitter bars during a test at 10 m/s (unconstrained-rubber): (a) experimental and (b) calculated.....	6
Figure 3. (a) Experimental and (b) calculated stress on ceramic: (c) experimental and (d) calculated stress on composite (unconstrained-rubber, $V = 10$ m/s).....	7
Figure 4. Stress on the incident and transmitter bars during a test at 10 m/s (constrained-rubber): (a) experimental and (b) calculated.....	8
Figure 5. Stress on the specimen (constrained-rubber) tested at 10 m/s: (a) experimental and (b) calculated stress on ceramic: (c) experimental and (d) calculated stress on composite.....	9
Figure 6. Stress measured on the incident and transmitter bars during a test at 16 m/s: (a) unconstrained rubber and (b) constrained rubber.....	10
Figure 7. Experimental data from ceramic/rubber/composite tested at 16 m/s. Stress measured on (a) ceramic and (b) composite. ....	10
Figure 8. Calculated output from strain gages on the incident and transmitter bars during a test at 16 m/s: (a) unconstrained rubber and (b) constrained rubber.....	11
Figure 9. Calculated data from ceramic/rubber/composite ( $V = 16$ m/s). Stress measured on (a) ceramic and (b) composite.....	11
Figure 10. Stress on the incident and transmitter bars during a test at 20.5 m/s on an unconstrained ceramic/rubber/composite: (a) experimental and (b) calculated. ....	12
Figure 11. Stress measured on ceramic: (a) experimental and (b) calculated. Stress measured on composite: (c) experimental and (d) calculated (unconstrained-rubber, $V = 20.5$ m/s). ....	13
Figure 12. Stress measured on the incident and transmitter bars during a test at 20.5 m/s on a constrained ceramic/rubber/composite: (a) experimental and (b) calculated. ....	14
Figure 13. Stress measured on ceramic: (a) experimental and (b) calculated: Stress measured on composite: (c) experimental and (d) calculated (constrained-rubber, $V = 20.5$ m/s). ....	15

---

## List of Tables

---

Table 1. Material properties used in finite element models.....	5
---	---

---

## **Acknowledgments**

---

The authors gratefully acknowledge financial support for this research under the Composite Materials Research Collaborative Program sponsored by the U.S. Army Research Laboratory, contract number DAAD19-01-2-0001.

INTENTIONALLY LEFT BLANK.

---

## 1. Introduction

---

Thick-section composite materials are frequently used under dynamic loading conditions, but their behavior is still not clearly understood. Impact loading of monolithic laminates has been the subject of several investigations, e.g., with glass/epoxy and graphite/epoxy (*1–10*). Similarly the penetration or perforation of composites has also been studied (*11, 12*), but severe complications arose whenever widely dissimilar materials were in intimate contact because their differing impedances caused complex wave reflection and transmission phenomena at each interface encountered. Thick, layered, or graded structures have significant potential for armor applications, and Li et al. (*13*) reported the dynamic characterization of layered and graded structures under impulsive loading. Another example of multilayer materials is provided by modern integral composite armor for vehicle applications as described by Fink (*14*) and Gama et al. (*15–17*). The armor material must provide ballistic protection at minimum weight and may contain several layers of different impedance, usually a ceramic layer followed by a thick composite plate (e.g., glass fiber/epoxy). High-velocity impact of this type of integral armor has been the subject of finite element studies by Mahfuz et al. (*18*). Jovicic et al. (*19*) modeled the ballistic behavior of gradient design composite armors.

The elastic adhesives used in composite armors can also alter wave propagation in the armor components. The mechanical behavior of different elastic adhesives under impact loads was studied by Martinez et al. (*20*) who reported that the capability of transmitting and reflecting the impact energy depends on the thickness and the type of the adhesive used. They concluded that the utilization of a thin layer of a rigid adhesive was the best way to transmit energy with the lowest reflection coefficient.

A central concept in enhancing the ability of multilayer material structures to withstand rapid impulsive loading is to spread the local impact load as rapidly and widely as possible. This can be achieved by placing a high wave-speed layer in the layered system. Gupta and Ding (*21*) studied numerically the effects of wave speed, layering geometry, and mechanical properties of the layer and substrate on load spreading. They showed that for a fixed layer thickness, a single thick high-strength high wave-speed layer appears to be able to offer the best lateral load spreading through intense and rapid wave transmission and spreading. The low wave-speed material used in multilayered targets appears to deteriorate the load spreading capability of the layered system.

Design of efficient multilayer materials for impact resistance requires both modeling and experimental efforts, and the split-Hopkinson pressure bar (SHPB) is a convenient tool in the latter respect although conventional data reduction routines obviously cannot be used for these materials. Two- and three-dimensional (2-D and 3-D) wave propagation in Hopkinson bar tests

has been investigated numerically by several authors (22, 23). In experimental studies, impact velocity of the striker bar and axial strain on the bar surfaces are the most commonly measured quantities. In numerical studies, besides the parameters previously mentioned, displacement and velocity of nodes, strain and stress of the elements, and interface forces can all be acquired as a function of time (24).

Prior work (25) addressed the situation with three different layers consisting of ceramic, rubber and composite, in which lateral expansion of the rubber was permitted. However, in practical large-scale structures, the rubber interlayer would be constrained by the surrounding material, and this present report considers the effects of such lateral constraint on the resulting properties. Samples used in SHPB testing can, at the most, have the same diameter as the bar, and earlier experiments showed that considerable radial flow occurred in the rubber interlayer. Larger samples, typical of many anticipated applications, would be subjected to severe lateral constraints which would, in turn, affect the through-thickness stresses reported. In fact, the real case will probably lie somewhere between the extremes of completely constrained and completely unconstrained interlayers, so the evaluation of both limiting cases is correspondingly important.

The effect of lateral constraint on ballistic performance has been investigated by many authors, and it is now well known that a compressive prestress is helpful in improving the fracture energy and impact resistance in brittle materials. Espinosa et al. (26) experimentally studied the impact resistance of ceramics confined in steel fixtures and showed the enhancement of ballistic efficiency of the confined ceramics. Martinez et al. (20) have determined the stress-strain curve of confined adhesive used in armor at high strain rates. Within the armor, elastic adhesives, comparable with the rubber interlayer in our case, were used to bond two large plates of much more rigid materials, which themselves impede subsequent lateral displacements of the adhesive.

This study, then, presents the initial results of a combined experimental and numerical investigation and serves to delineate the principal features and identify the problems to be solved in order to develop a better understanding of the effects of constraint in such multilayer materials.

---

## **2. Experiments and Modeling**

---

Samples were prepared from multilayer plates with layers of widely different impedances. The plates consisted of three layers, namely a 13.96-mm-thick alumina ceramic, a 1.5-mm-thick layer of ethylene propylene diene monomer (EPDM) rubber, and a layer of glass/epoxy composite.

The  $5 \times 5$  plain weave S-2 Glass\* fiber woven fabric ( $0.814 \text{ kg/m}^2$ ) SC15† epoxy (toughened resin) composite plates were 11.3-mm-thick and were produced using the vacuum-assisted resin transfer molding process. Lateral confinement of the rubber interlayer was obtained by placing a 6-mm-wide steel retaining ring around the junction of the sample as illustrated in figure 1. An interference fit was achieved between the rubber and the steel ring, and no rubber was squeezed out into the region between them while testing. Possible inertial effects and interactions between the ring and the other components of the sample were checked via tests on individual ceramic and composite samples with the ring in place. No modification to the wave propagation behavior was observed in the presence of the steel ring. The ceramic layer was always at the impacted side.

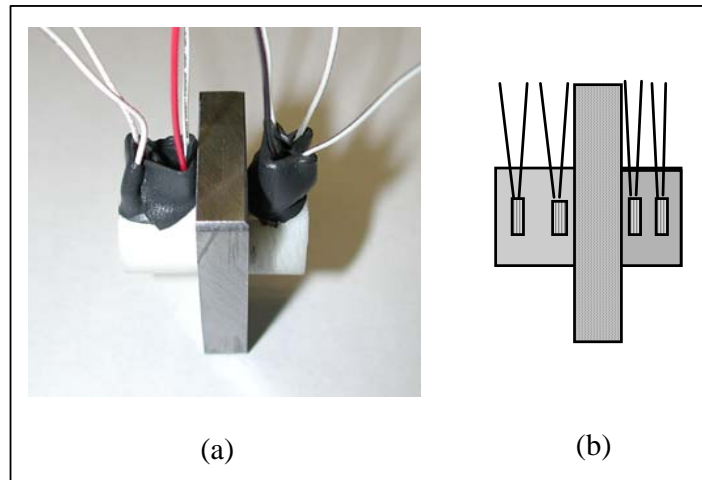


Figure 1. (a) Constrained sample prior to testing and (b) schematic of setup.

Cylindrical samples, 15.7 mm in diameter, were core drilled from the plates in the through-thickness direction. Samples were compression tested over a wide range of displacement rates using the SHPB apparatus (the compression axis normal to fiber plane). However, the focus of the present report concerns a series of tests, all of which were conducted with striker bar velocities of 10, 16, or 20.5 m/s—as an approximate guide, these velocities would generate “average strain rates” of  $\sim 400$ , 500, and 700/s, respectively.

The particular SHPB apparatus used consists of Inconel‡ 718 bars, a 356-mm-long striker bar, 3450-mm incident, and 1850-mm transmitter bars, all with a diameter of 19 mm. Further details of the experimental setup and standard data reduction routines are available elsewhere (27). Samples were fitted with strain gages, as shown in figure 1, so as to monitor real-time strains/stresses during the course of the tests. Strain gages with 0.79-mm element lengths were

\*S-2 Glass is a registered trademark of Owens Corning.

†SC15 is a trademark of Applied Poceramic Incorporation..

‡Inconel is a registered trademark of the INCO family of companies.

used generally, although several tests were also carried out with an array of gages designed to sample the strain simultaneously at several locations along the sample length and thus provide a strain/time/position map of the wave passage.

A 3-D SHPB finite element model was used to study stress wave propagation in the multilayer materials and also in the individual components. Rubber is a highly nonlinear elastic material and the role of this nonlinear material has been studied by modeling the rubber layer with experimentally determined material data. The analyses were performed using a commercial explicit finite element code LS-DYNA 960. Two axes of symmetry were assumed, so only one quarter of the bar was modeled. For each test modeled, the output was displayed at several locations, within the sample as well as at the location of the strain gages on the incident and transmitter bars of the SHPB apparatus. The desired ideal result is that output from the strain gages on the incident and transmitter bars closely match data calculated from the model. Similarly, output measured by gages on the sample should also closely match data calculated from the model. When both these conditions are met, it indicates that the model is accurately capturing the wave propagation behavior in the sample and bars.

The model has four components in contact: a striker bar of 356 mm in length, an incident bar and a transmission bar each of 1524 mm in length, and the specimen, i.e., the ceramic, rubber, and composite layers, the thicknesses of which are 14, 1.5, and 10.6 mm, respectively. The bar diameter is 19.05 mm, and the diameter of the specimen is 16.0 mm. The component materials are modeled with 8-node solid elements, and the interfaces are modeled with the automatic contact sliding interfaces without friction. The impact velocity of the striker bar ( $V = 10, 16, \text{ and } 20.5 \text{ m/s}$ ) has been defined as the initial condition, and all other boundaries are traction free and can move in any direction. In order to save computation time, the simulation uses bars 1524 mm in length, instead of full length bars. It will be seen later from the figures that this has the effect of decreasing the transit time between successive waves and shortening the wave duration slightly, however, it does not affect the basic wave shapes or amplitudes. A few trial computations were carried out using full-length bars, but apart from the slightly smaller time window, no significant differences were found, and the shorter bars were used henceforth.

Material properties used in the finite element code are shown in table 1. The ceramic was modeled with an isotropic elastic material model, and the composite was modeled with an orthotropic elastic material. Rubber was modeled with two different material models. The Mooney-Rivlin Model (28) (two parameter nonlinear material model) was used for the unconstrained configuration and the Blatz-Ko Material Model (28) was used for the constrained configuration. The Blatz-Ko Material Model shows better agreement for the hydrostatic state of stress of the rubber. For the unconstrained case, the rubber interlayer deforms very extensively, and this large deformation caused stability problems in the finite element model. This problem was solved by using different material parameters for the different cases. While higher shear modulus values give better results for the constrained case, in unconstrained samples, the lower shear modulus values give better agreement with the experimental results. Actual compression

tests on the rubber itself confirm that this behavior is indeed observed in practice. To be able to use the same material model would probably be preferable, and this will be implemented for future simulations. The Inconel bars were modeled with an isotropic elastic material model, and lateral confinement of the rubber interlayer was modeled by preventing the displacements in both x and y directions for this component.

Table 1. Material properties used in finite element models.

Material	Modulus of Elasticity (GPa)	Poisson's Ratio	Density (kg/m <sup>3</sup> )	Other
Ceramic	370	0.22	3900	—
Mooney-Rivlin rubber	—	0.495	1200	A:0.2 (MPa) B: 0.8 (MPa)
Blatz-Ko rubber	—	0.493	1200	G: 20 (MPa)
Composite	E <sub>1</sub> : 40 E <sub>2</sub> : 40 E <sub>3</sub> : 15	v <sub>21</sub> : 0.12 v <sub>31</sub> : 0.173 v <sub>32</sub> : 0.173	1668	G <sub>1</sub> : 8 (GPa) G <sub>2</sub> : 8 (GPa) G <sub>3</sub> : 8 (GPa)
Inconel	207	0.3	7850	—

### 3. Results

The experimental results are presented here in order of increasing incident bar velocity which corresponds to increasing loading rate and, as will become clear, increasing degrees of damage within the samples. Three different striker bar velocities were used, and SHPB tests and simulations were performed for both the unconstrained and the constrained situations. The primary data for each test consist of (1) experimental output from the SHPB bars for constrained and unconstrained specimens, (2) measured strain gage data from each sample, and (3) numerical data, which are then compared with the corresponding experiments.

#### 3.1 Impact Velocity (10 m/s)

Figure 2 shows experimental and calculated SHPB data from an unconstrained sample tested at a striker bar velocity of 10 m/s, and close agreement is noted between the experimental and numerical results. Experimentally, it is seen that the transmitted wave amplitude slowly increases to ~60 MPa as indicated and exhibits a minor peak of ~100  $\mu$ s before that. Calculated data show almost identical behavior.

Experimental data from the ceramic portion of an unconstrained strain-gaged sample are shown in figure 3a, while figure 3b shows the corresponding numerical data. The insets in the figure indicate the location of the gages or nodes interrogated. First, it is noted that the stress varies greatly with time and, second, it is noted that the stress close to the incident bar/ceramic interface

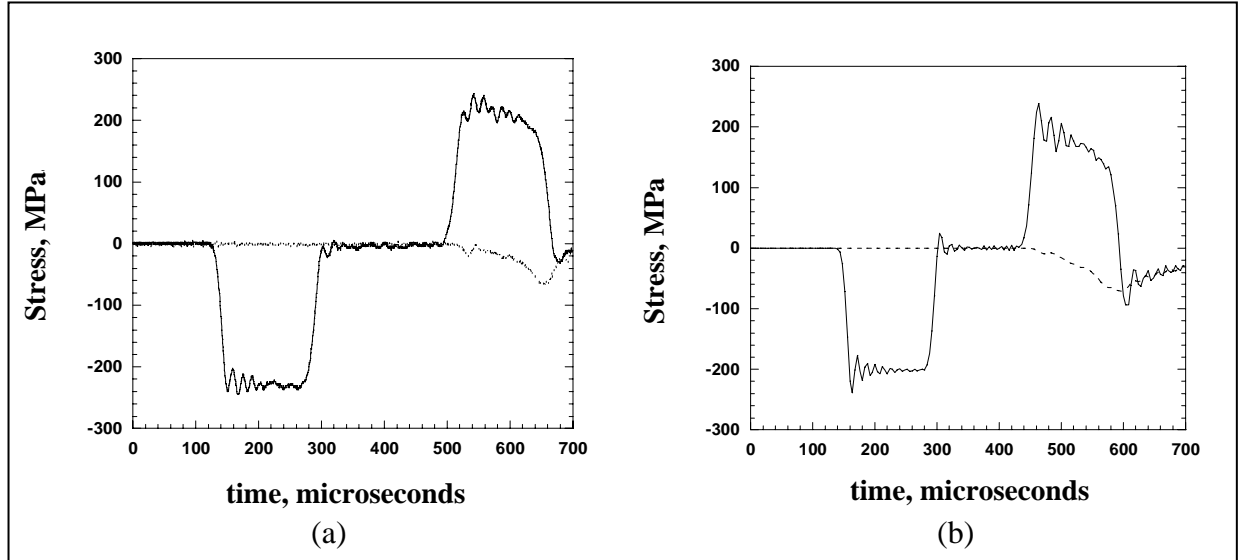


Figure 2. Stress on the incident and transmitter bars during a test at 10 m/s (unconstrained-rubber): (a) experimental and (b) calculated.

is invariably greater than that closer to the ceramic/rubber interface. Similarly, figure 3c and d shows experimental and calculated stresses measured on the composite portion of the sample.

Note that the magnitude of the initial peak in the composite layer is less than that in the ceramic layer and, again, an inhomogeneous stress distribution exists. Also, fewer large stress oscillations are noted than in the case of the ceramic. Generally, the numerical data show broadly similar behavior to the experimental data in each case, including multiple peaks in the ceramic, similar scale of stress inhomogeneity, similar magnitudes of the maximum stress, and a similar overall shape to each stress vs. time curve.

Figure 4 shows experimental and numerical SHPB data from a sample, tested at a striker bar velocity of 10 m/s, in which the rubber interlayer was constrained. Comparison with corresponding unconstrained data (figure 2a and b) shows that constraint greatly modifies the reflected and transmitted wave shapes. The constrained sample exhibits a maximum transmitted wave amplitude of  $\sim 200$  MPa as compared to  $\sim 60$  MPa for the unconstrained case. Figure 5 shows experimental and calculated stresses within the ceramic and composite, as a function of time, at different locations within the sample. It shows significantly different behavior compared to the unconstrained data, namely, what is essentially a single peak in the ceramic and composite and a more rapidly rising stress in both of the components when the rubber interlayer is constrained. The peak stress values in each component are almost the same value, i.e.,  $\sim 250$  MPa—considerably higher than when the rubber is unconstrained.

### 3.2 Impact Velocity (16 m/s)

When tested at an intermediate velocity, samples began to suffer limited damage, although none failed catastrophically. Lateral constraint of the rubber interlayer was found to increase the

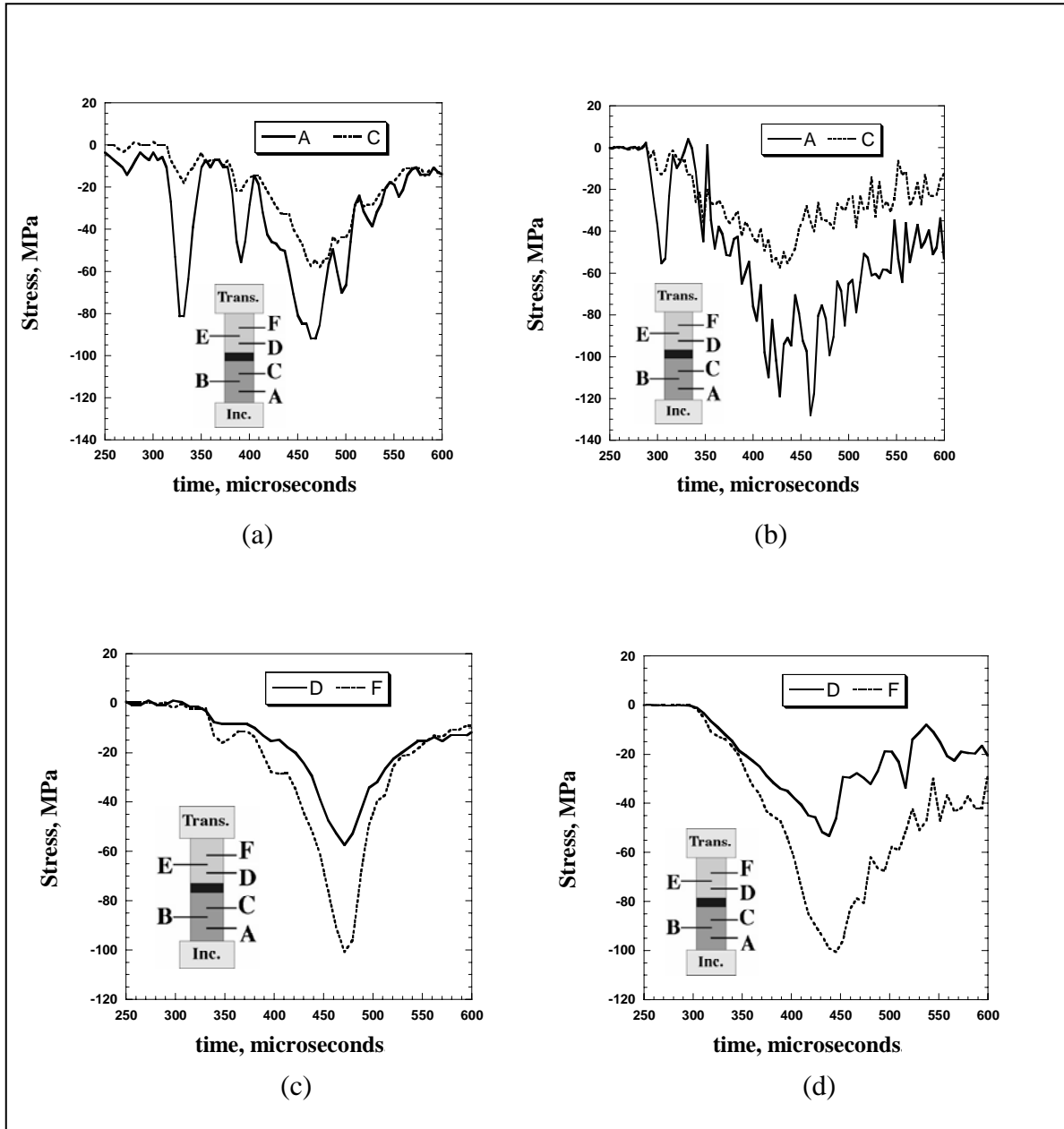


Figure 3. (a) Experimental and (b) calculated stress on ceramic: (c) experimental and (d) calculated stress on composite (unconstrained-rubber,  $V = 10$  m/s).

damage level in both of the components. Visual damage in the composite exhibited itself as lateral spreading of the layers accompanied by significant radial strain, whereas the ceramic only exhibited occasional and limited spalling from the edges of the impacted face.

Figure 6a and b shows experimental SHPB data for the trilayer ceramic/rubber/composite with the rubber layer unconstrained and constrained, respectively. It is clear that the shapes of the transmitted and reflected waves for the constrained configuration are drastically different from the unconstrained case.

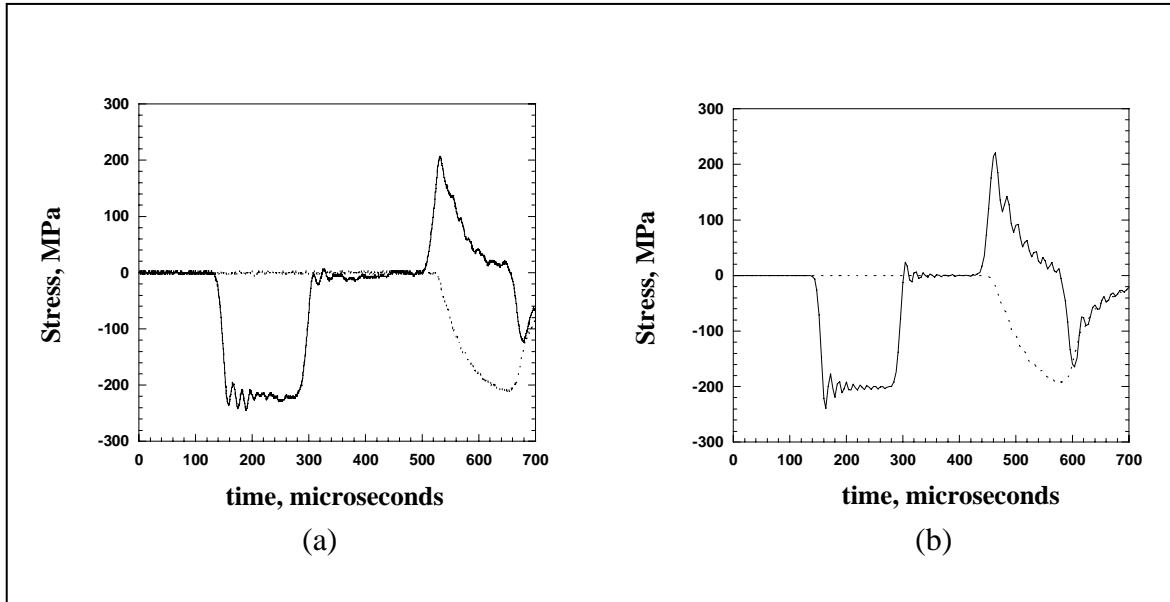


Figure 4. Stress on the incident and transmitter bars during a test at 10 m/s (constrained-rubber): (a) experimental and (b) calculated.

Major differences in the wave propagation characteristics, caused by lateral confinement of the rubber interlayer, are also clearly demonstrated in strain gage data collected from the separate layers. Figure 7a and b shows experimental data from the ceramic and composite layers, respectively. Data from gages on the ceramic show a marked increase in the measured stress levels resulting from confinement (figure 7a). Nevertheless, the general complexity of the wave forms of the unconstrained sample remains reminiscent of those tested at lower velocity (see figure 3a) insofar as three peaks may be discerned at  $\sim 65\text{-}\mu\text{s}$  intervals. The peaks present in the unconstrained case merge into essentially one peak when the rubber is constrained. In the composite, the maximum stress level experienced with constraint of the rubber interlayer is  $\sim 2.5\times$  that for the unconstrained sample (figure 7b), while the corresponding stress in the ceramic increases by a factor of  $\sim 3.3$ .

Figure 8a and b shows the calculated data from the Hopkinson bars. For these samples, agreement between the experimental (figure 6a and b) and numerical data is currently slightly less close than for the low-velocity case, principally because damage has begun to occur in the experimental samples, but damage mechanisms have not yet been included in the present model, although they have been discussed elsewhere (29). The effect of damage initiation is reflected in a truncation of the early peak in the measured reflected wave.

Figure 9a and b shows numerical data from the individual ceramic and composite layers for the constrained and unconstrained cases. The elements chosen for the numerical data were at approximately the same position as the strain gages reported in figure 7. Comparison of these two figures shows that the calculated stress magnitudes are very similar to the experimental

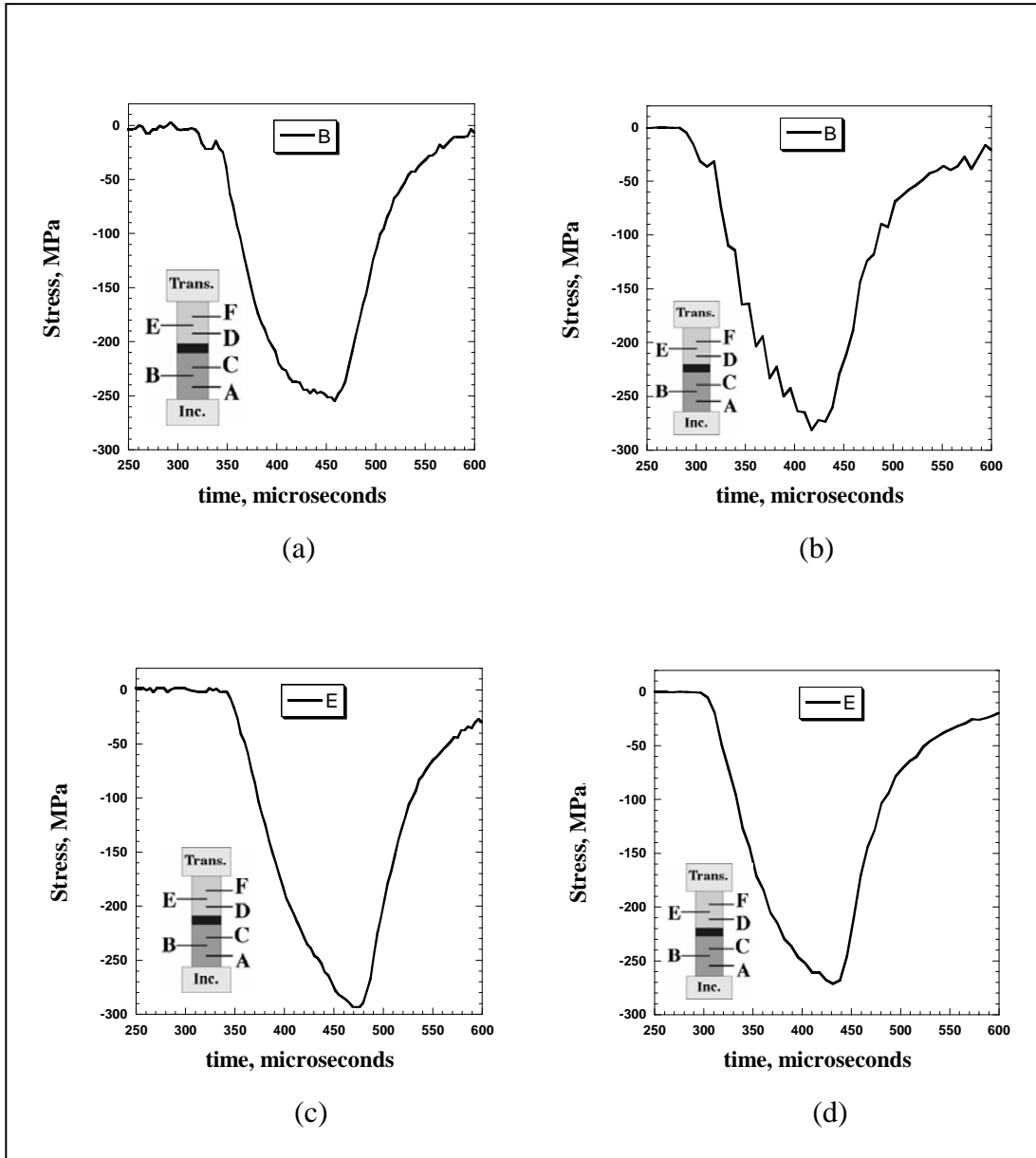


Figure 5. Stress on the specimen (constrained-rubber) tested at 10 m/s: (a) experimental and (b) calculated stress on ceramic: (c) experimental and (d) calculated stress on composite.

values. They differ only very slightly in detail as a result of the slight “stress-averaging” effect due to the finite size of the gages and, despite this, the same general shapes are found.

### 3.3 Impact Velocity (20.5 m/s)

A similar set of experiments and simulations was then carried out for a higher striker bar velocity. Now the presence of the rubber interlayer and its constraint leads to major differences in the wave propagation characteristics. Figure 10a and b shows experimental and calculated data from the incident and transmitter bars for the unconstrained rubber case. For this configuration, the basic shapes and magnitudes of the transmitted waves resemble each other, but

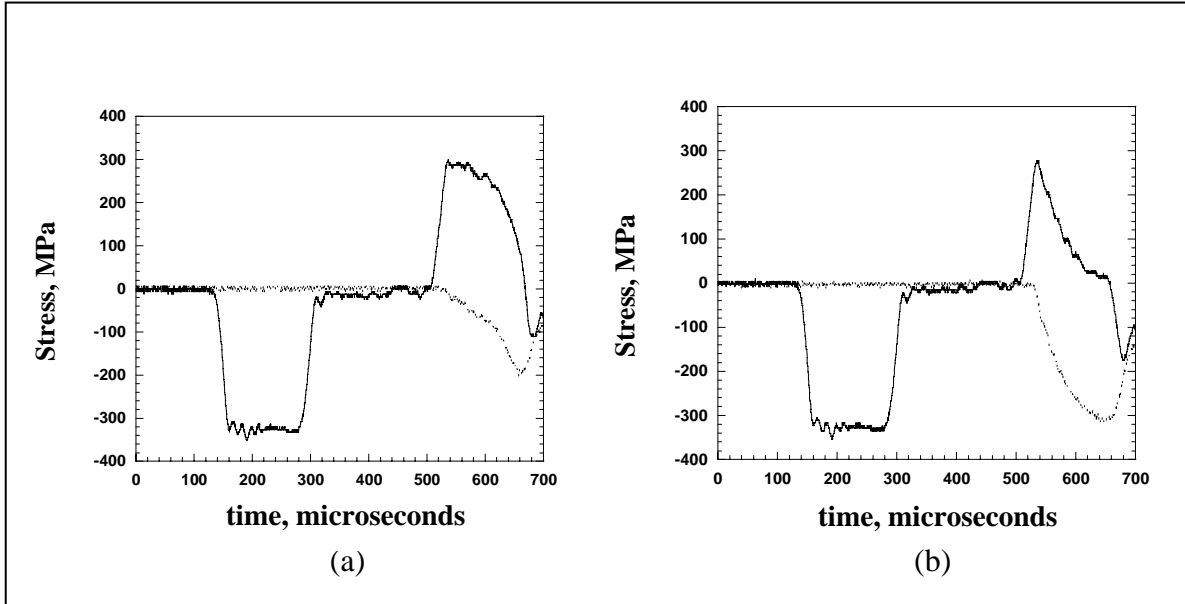


Figure 6. Stress measured on the incident and transmitter bars during a test at 16 m/s: (a) unconstrained rubber and (b) constrained rubber.

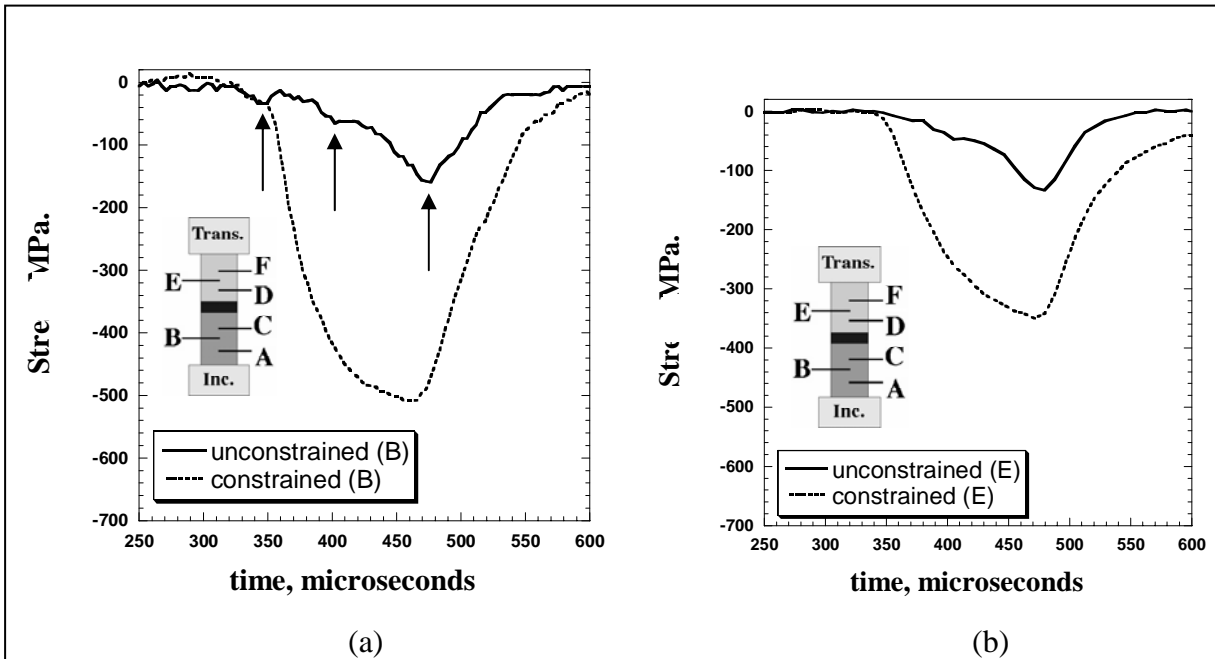


Figure 7. Experimental data from ceramic/rubber/composite tested at 16 m/s. Stress measured on (a) ceramic and (b) composite.

it is evident that significant physical damage begins to occur during the test at a stress of ~400 MPa, most clearly indicated by a change in the reflected wave shape.

Figure 11 shows experimental and numerical data from the individual ceramic and composite layers, respectively, with an unconstrained rubber interlayer. Figure 11a and c shows the actual

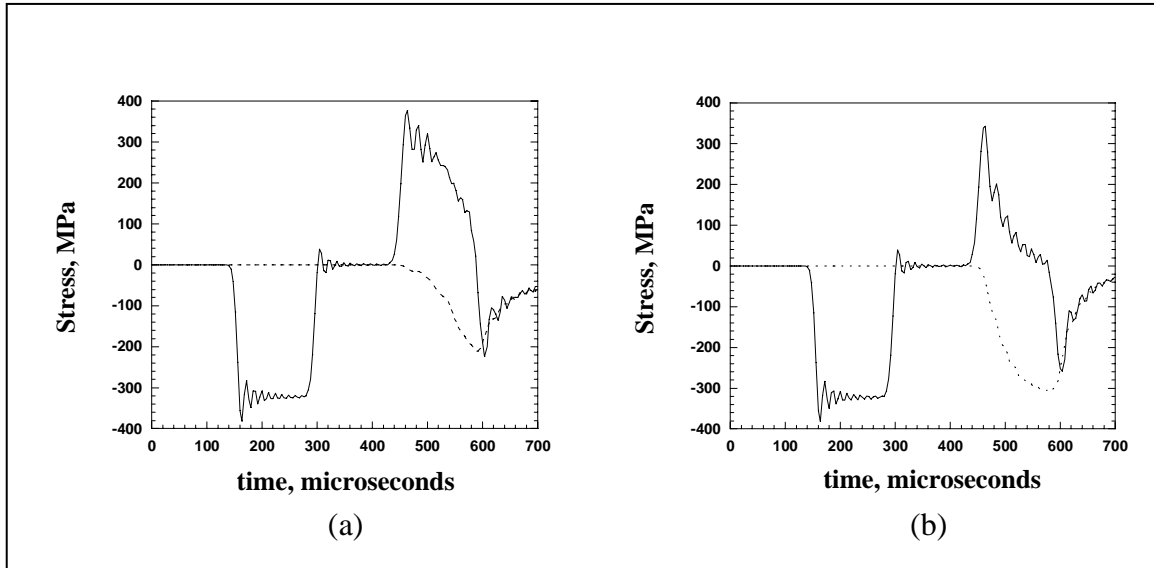


Figure 8. Calculated output from strain gages on the incident and transmitter bars during a test at 16 m/s: (a) unconstrained rubber and (b) constrained rubber.

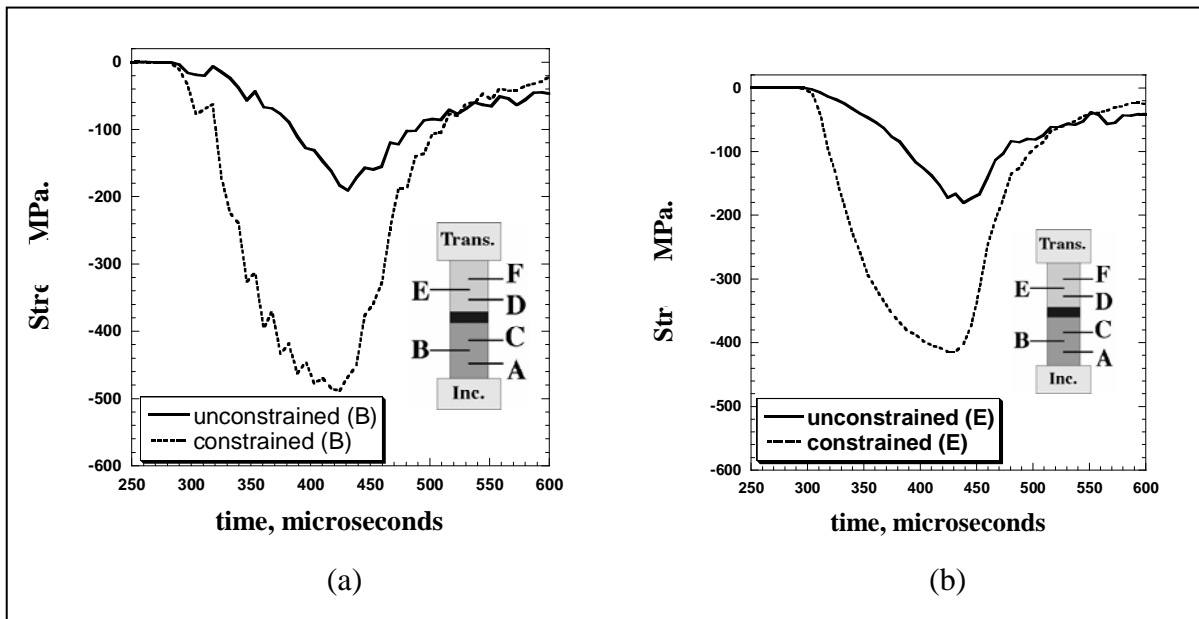


Figure 9. Calculated data from ceramic/rubber/composite ( $V = 16$  m/s). Stress measured on (a) ceramic and (b) composite.

stress measured from two strain gages close to incident bar and rubber interfaces of the sample for the ceramic and, similarly, for the composite. (During this particular experiment, the gage close to the transmitter bar interface on the composite broke off due to the high strain at this location. As a result, only the initial portion of the stress read-out can be recorded for this gage.) Figure 11b shows the z-stress in the ceramic layer, calculated at two elements, at almost the same

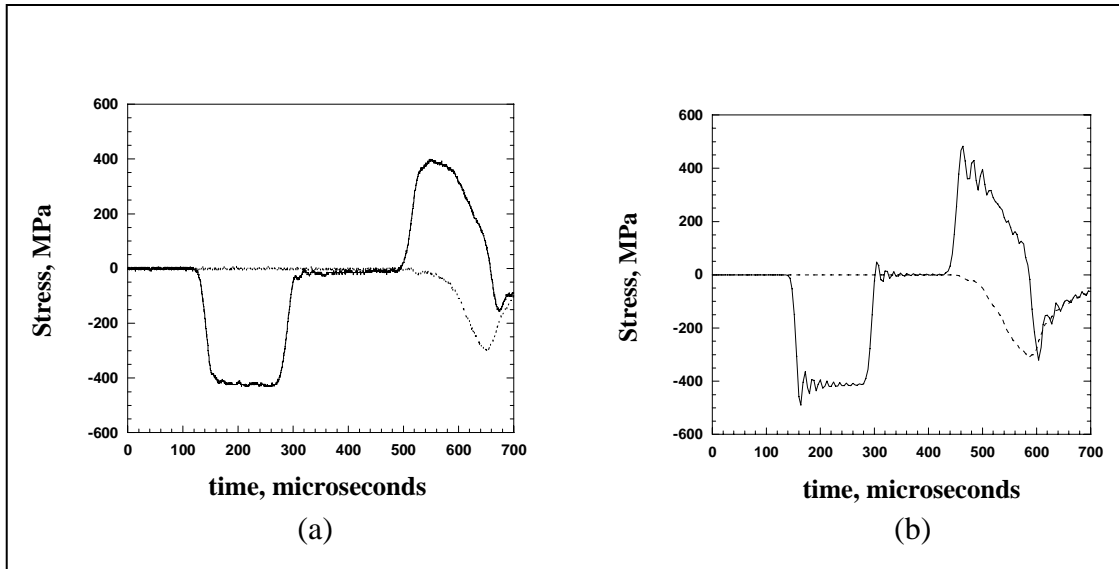


Figure 10. Stress on the incident and transmitter bars during a test at 20.5 m/s on an unconstrained ceramic/rubber/composite: (a) experimental and (b) calculated.

location as the experimental case. It can be clearly seen that during the course of testing the material experiences a nonuniform stress distribution, with the minimum occurring close to the rubber interlayer. Figure 11d shows calculated data from a similar element on the composite layer. Despite possible limitations of the present model due to damage initiation, it is seen that the calculated maximum stress levels are still very close to the measured stresses.

Figure 12a and b shows measured and calculated data from the incident and transmitter bars for the constrained rubber case. For these samples, agreement between the experimental and numerical data is again less close than for the unconstrained case at lower striker bar velocities (figures 6b and 8b) and the peak value of the reflected pulse has again been somewhat overestimated.

Figure 13 presents experimental and numerical data from the individual ceramic and composite layers. Figure 13a and c shows the actual stress measured from a single strain gage at midlength of the sample for the ceramic and composite. Similarly, figure 13b and d shows numerical data from the individual ceramic and composite layers at comparable locations. Comparison with figure 11 shows that a major effect of constraint is to broaden the principal peaks, resulting in the components remaining longer at these higher stress levels. The maximum stress is still experienced in each case ( $\sim 140 \mu\text{s}$ ) after the initial impact. Even for this high-impact velocity, the model still captures the general features of wave propagation and the form of stress distribution. The agreement in terms of absolute values of stress can also be clearly seen from the figures.

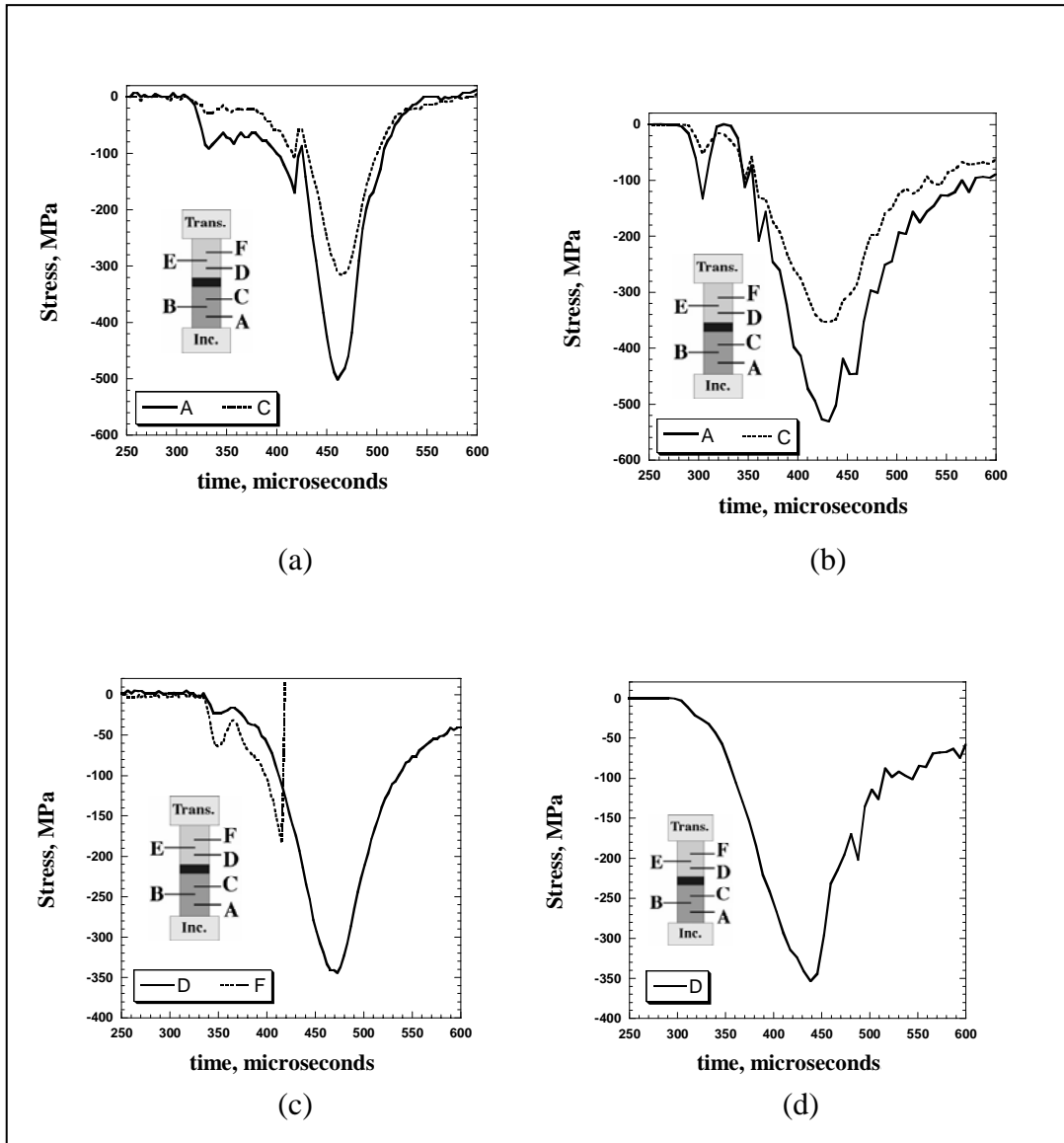


Figure 11. Stress measured on ceramic: (a) experimental and (b) calculated. Stress measured on composite: (c) experimental and (d) calculated (unconstrained-rubber,  $V = 20.5$  m/s).

## 4. Discussion

The main objective of the present work was to investigate experimentally and numerically the effects of lateral confinement of the rubber interlayer on the wave propagation characteristics of the multilayer material over a range of impact velocities. The SHPB is a convenient tool for high strain rate testing of homogeneous elastic/plastic materials, but direct interpretation of SHPB data is not possible for materials which are nonlinear or of very low or very high

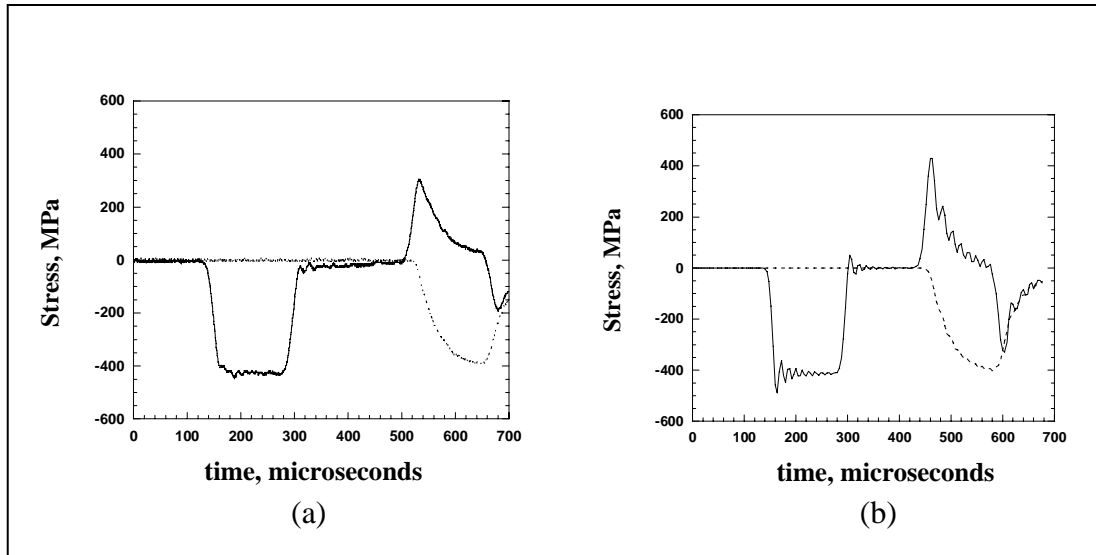


Figure 12. Stress measured on the incident and transmitter bars during a test at 20.5 m/s on a constrained ceramic/rubber/composite: (a) experimental and (b) calculated.

impedance relative to the bars, or anisotropic, or composed of several layers of distinctly different materials as in the case studied here. However, if numerical simulation procedures can be developed which satisfactorily reproduce the output data of SHPB tests, then (a) the tests themselves can be better interpreted and (b) simulations can be carried out with increased confidence.

A previous study (25) showed that there was excellent agreement between numerical data and actual data measured from the incident and transmitter bars for a two-layer ceramic/composite test. That model satisfactorily captured the details of wave transmission. The present three-layer model also satisfactorily captures the details of wave transmission, the general features of wave propagation, stress magnitudes, and the form of stress distribution, and consequently offers considerably enhanced insight into the processes leading to damage generation in such multilayer materials.

The experiments are subject to some limitation because the strain gages average the data over their active gage length, which is typically 0.79 mm as compared with ~0.4 mm for the element size in the model. Also, the measured stress is seen to be very strongly dependent upon the exact placement of the gage within the specimen length. Finally, some of the strain gages mounted on the components could not record all the stress wave history either because of their failure or because of the high strain levels generated in the components (see figure 11c).

Keeping these limitations in mind, it can be appreciated that there is nonetheless good agreement between experimental and numerical data even for the highest impact velocity tests. For example, figure 3a shows experimental data from two gages (5 mm apart) on the ceramic sample

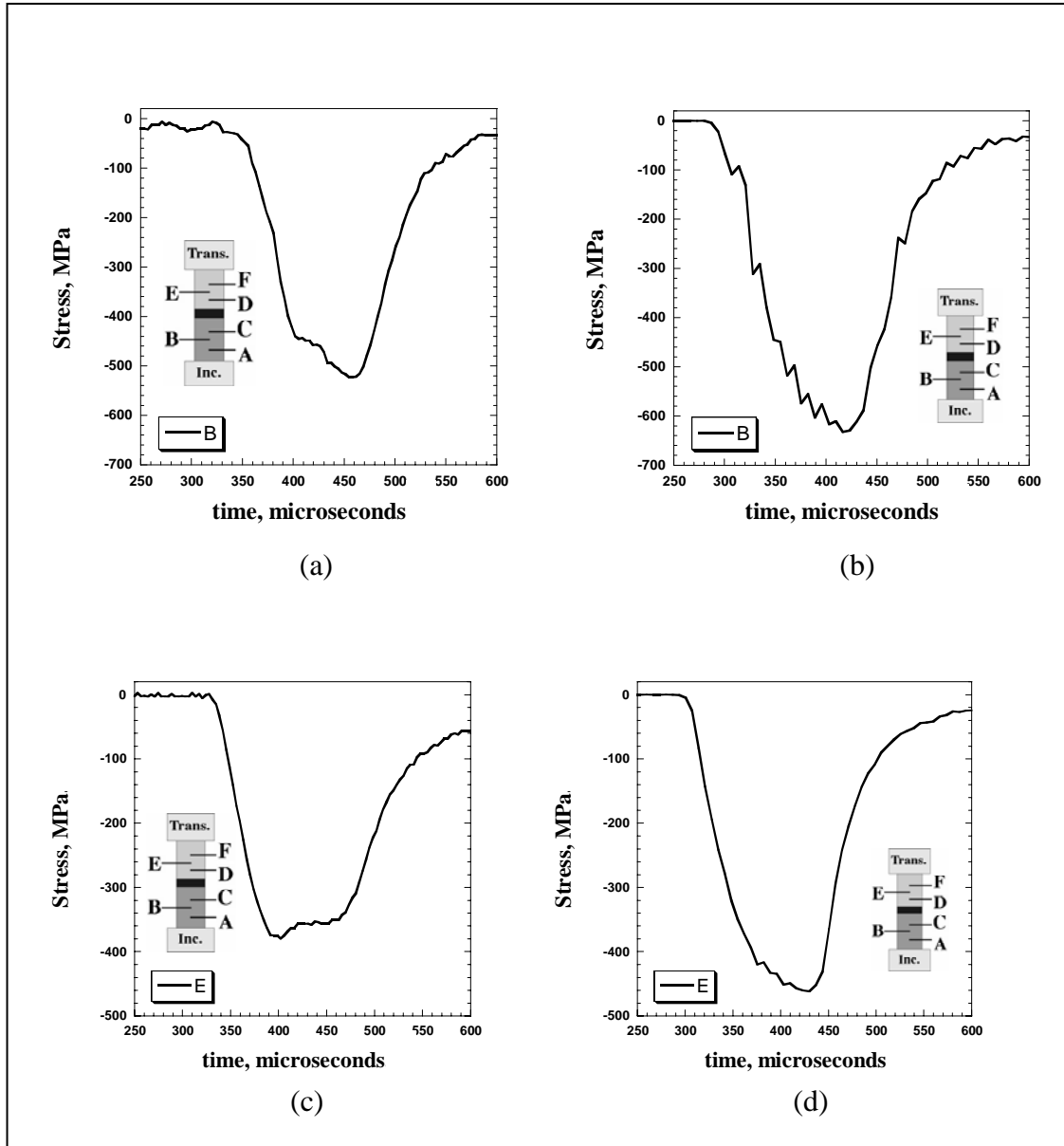


Figure 13. Stress measured on ceramic: (a) experimental and (b) calculated: Stress measured on composite: (c) experimental and (d) calculated (constrained-rubber,  $V = 20.5$  m/s).

surface. After the initial stress peak, a second major peak is observed  $\sim 150 \mu\text{s}$  later; the numerical data (figure 3b) likewise show the initial and second peak stresses at approximately similar intervals. Furthermore, interpolating to comparable elemental positions, the relative magnitudes are quite similar. The absolute magnitudes of the maximum measured stresses are, however, slightly different, and this is partially due to reasons of data source location and the “averaging” effect of the strain gage size previously mentioned.

Throughout all the current sets of experiments and simulations, close agreement was achieved between the model and experiment. Figures 6a and b and 8a and b show experimental and

calculated data from the Hopkinson bars. Again, the data match closely, showing that LS-DYNA accurately captures the details of wave propagation.

A major conclusion from the present results is that constraint of the rubber layer drastically alters the response of the material, and this is most easily demonstrated by the change of the reflected and transmitted wave shapes. For example, in the case of the lowest velocity tests, instead of reaching a maximum transmitted stress of ~60 MPa, as for the unconstrained case, the maximum stress is ~210 MPa when constrained (compare figures 2a and 4a). Also the stress rises relatively faster and more uniformly for the second case: basically, lateral confinement of the rubber interlayer increases the wave transmission efficiency between the components.

It can also be seen that the shapes of the wave traveling through the individual ceramic and composite layers are widely different in the unconstrained material, an observation that is confirmed both by experimental measurements and numerical analysis. For example, figure 3 shows that an almost instantaneous and rapid stress increase occurs for the ceramic, followed by further major oscillations, while the composite shows a largely monotonic and gradual increase in stress level. By contrast, in constrained samples, the wave shapes are almost the same for the ceramic and composite (see figure 5) and come to resemble the shape of the wave traveling in the composite. In other words and in common with many other kinetic processes, the component of lowest impedance dominates the process.

Rubber leads to a highly inhomogeneous stress distribution within the components when it is constrained. Generally, the part of the sample close to the unconstrained rubber experiences a reduced stress while the remainder may experience a much higher stress level. However, when the rubber is constrained, the differences in stress level within the components are greatly reduced, although the stress is still by no means homogeneous.

For the higher velocity tests, agreement between the experimental and numerical data is currently slightly less close than for the lower velocity cases (see figures 10–13), for reasons associated with damage evolution. During testing at high velocities, the ceramic frequently shattered, and various damage modes were activated in the composite. Even though the material models used in this study do not include failure parameters, the numerical calculations still capture the general features of wave propagation and the form of stress distribution. Obviously, further refinement along these lines will significantly improve agreement between experiment and model.

In this respect, the present work indicates several avenues for characterizing damage evolution in these, or similar materials at high strain rates since the effects of damage are clearly indicated in the output signals. For example, the principal differences between figures 4a and 10a can be ascribed to the onset of significant damage that alters the (here assumed elastic) properties of the materials. Therefore, the point at which experimental and numerical data begin to diverge probably defines the point at which significant damage begins. It is thus possible to study, by comparison of experimental and numerical data, damage evolution at high strain rate indirectly as a function of strain and strain rate. When coupled with microscopic examination of recovered

material, the present type of data would elucidate the processes and sequence of deformation and fracture events.

This is potentially of great utility because failure criteria are included in recent material models, but a definition of stress and strain levels associated with these events is presently rather imprecise. So, if stress or strain levels associated with the onset of various damage mechanisms can be determined, these could be inserted into the numerical models and provide improved accuracy.

---

## **5. Conclusions**

---

The present work has demonstrated the feasibility of modeling stress wave propagation in complex multilayer materials. It has been shown that the effects of confinement of normally low modulus materials can significantly affect their response to wave propagation. Severe stress inhomogeneities and discontinuities may exist in multilayer materials, and these may have serious consequences for the mechanical and other properties. Numerical modeling clearly shows that during Hopkinson bar testing of multilayer materials, stress is not distributed uniformly inside the specimen. The one-dimensional stress state usually assumed for conventional SHPB testing is questionable, and for a complete understanding of the wave propagation, both numerical and experimental results have to be coupled. In this study, both methods were used, and the stress states inside the components were presented. Accuracy will be increased, especially for the high pressure levels, by implementing damage parameters in future material models.

---

## 6. References

---

1. Lee, S.; Sun, C. Dynamic Penetration of Graphite-Epoxy Laminates Impacted by a Blunt-Ended Projectile. *Composites Science and Technology* **1993**, *49* (4), 369–380.
2. Goldsmith, W.; Dharan, C.; Chang, H. Quasi-Static and Ballistic Perforation of Carbon-Fiber Laminates. *International Journal of Solids and Structures* **1995**, *32* (1), 89–103.
3. Wu, E.; Chang, L. Loading Rate Effect on Woven Glass Laminated Plates by Penetration Force. *Journal of Composite Materials* **1998**, *32* (8), 702–721.
4. Abrate, S. Modeling of Impact on Composite Structures. *Comp. Struct.* **2001**, *51*, 129–138.
5. Collombet, F.; Lalbin, X.; Bonini, J.; Martin, V.; Lataillade, J. L. Damage Criteria for the Study of Impacted Composite Laminates. *Composites Science and Technology* **1998**, *58* (5), 679–686.
6. Chen, W.; Ravichandran, G. Dynamic Compressive Failure of a Glass Ceramic Under Lateral Confinement. *Journal of the Mechanics and Physics of Solids* **1997**, *45* (8), 1303–1328.
7. DeLuca, E.; Prifti, J.; Betheney, W.; Chou, S. C. Ballistic Impact Damage of S-2 Glass-Reinforced Plastic Structural Armor. *Composites Science and Technology* **1998**, *58* (9), 1453–1461.
8. Gama, B. A.; Gillespie, J. W., Jr.; Mahfuz, H.; Raines, R. P.; Haque, A.; Jeelani, S.; Bogetti, T. A.; Fink, B. K. High Strain-Rate Behavior of Plain-Weave S-2 Glass/Vinyl Ester Composites. *Journal of Composite Materials* **2001**, *35* (13), 1201–1228.
9. Kim, J.; Kang, K. An Analysis of Impact Force in Plain-Weave Glass/Epoxy Composite Plates Subjected to Transverse Impact. *Composites Science and Technology* **2001**, *61* (1), 135–143.
10. Cantwell, W.; Morton, J. Geometrical Effects in the Low Velocity Impact Response of Cfrp. *Composite Structures* **1989**, *12* (1), 39–59.
11. Mines, R.; Roach, A.; Jones, N. High Velocity Perforation Behaviour of Polymer Composite Laminates. *International Journal of Impact Engineering* **1999**, *22* (6), 561–588.
12. Wen, H. Penetration and Perforation of Thick FRP Laminates. *Composites Science and Technology* **2001**, *61* (8), 1163–1172.

13. Li, Y.; Ramesh, K.; Chin, E. Dynamic Characterization of Layered and Graded Structures Under Impulsive Loading. *International Journal of Solids and Structures* **2001**, *38* (34, 35), 6045–6061.
14. Fink, B. Performance Metrics for Composite Integral Armor. *Journal of Thermoplastic Composite Materials* **2000**, *13* (5), 417–431.
15. Gama, B.; Bogetti, T. A.; Fink, B. K.; Yu, C. J.; Claar, T. D.; Eifert, H. H.; Gillespie, J. W., Jr. Aluminum Foam Integral Armor: A New Dimension in Armor Design. *Composite Structures* **2001**, *52* (3, 4), 381–395.
16. Gama, B.; Gillespie, J. W., Jr.; Bogetti, T.; Fink, B. Innovative Design and Ballistic Performance of Lightweight Composite Integral Armor. In *SAE 2001 World Congress*; SAE: Detroit, MI, 2001.
17. Gama, B.; Gillespie, J. W., Jr.; Mahfuz, H.; Bogetti, T.; Fink, B. Effect of Non-Linear Material Behavior on the Through-Thickness Stress Wave Propagation in Multi-Layer Hybrid Lightweight Armor. In *Advances in Comp. Eng. and Sci.*; Tech. Sci. Press: Palmdale, CA, 2000; Vol. I, pp. 157–162.
18. Mahfuz, H.; Zhu, Y. H.; Haque, A.; Abutalib, A.; Vaidya, U.; Jeelani, S.; Gama, B. A.; Gillespie, J. W., Jr. Investigation of High-Velocity Impact on Integral Armor Using Finite Element Method. *International Journal of Impact Engineering* **2000**, *24* (2), 203–217.
19. Jovicic, J.; Zavaliangos, A.; Ko, F. Modeling of the Ballistic Behavior of Gradient Design Composite Armors. *Composites Part A - Applied Science and Manufacturing* **2000**, *31* (8), 773–784.
20. Martinez, M. A.; Chocron, I. S.; Rodriguez, J.; Galvez, V. S.; Sastre, L. A. Confined Compression of Elastic Adhesives at High Rates of Strain. *International Journal of Adhesion and Adhesives* **1998**, *18* (6), 375–383.
21. Gupta, Y.; Ding, J. Impact Load Spreading in Layered Materials and Structures: Concept and Quantitative Measure. *International Journal of Impact Engineering* **2002**, *27* (3), 277–291.
22. Verleysen, P.; Degrieck, J. Improved Signal Processing for Split Hopkinson Bar Tests on (Quasi-)Brittle Materials. *Experimental Techniques* **2000**, *24* (6), 31–33.
23. Bacon, C. Separation of Waves Propagating in an Elastic or Viscoelastic Hopkinson Pressure Bar With Three-Dimensional Effects. *International Journal of Impact Engineering* **1999**, *22* (1), 55–69.
24. Gama, B.; Lopatnikov, S.; Gillespie, J. W., Jr. Numerical Hopkinson Bar Analysis: Validity of One-Dimensional Assumptions. *CD Proceedings, ASC 2003 Conference*, Gainesville, FL, 20–22 October 2003.

25. Tasdemirci, A.; Hall, I.; Gama, B.; Guden, M. Stress Wave Propagation Effects in Multi-Component Composite Materials. *Journal of Composite Materials* **2003**, 38 (12), 995–1011.
26. Espinosa, H. D.; Brar, N. S.; Yuan, G.; Xu, Y.; Arrieta, V. Enhanced Ballistic Performance of Confined Multi-Layered Ceramic Targets Against Long Rod Penetrators Through Interface Defeat. *International Journal of Solids and Structures* **2000**, 37 (36), 4893–4913.
27. Guden, M.; Hall, I. Dynamic Properties of Metal Matrix Composites: A Comparative Study. *Materials Science and Engineering A-Structural Materials Properties Microstructure and Processing* **1998**, 242 (1, 2), 141–152.
28. *LS-DYNA Keyword User's Manual Version 970*; Livermore Software Technology (LSTC) Corporation: Livermore, CA, 2003.
29. Yen, C. F. Ballistic Impact Modeling of Composite Materials. In *7th International LS-DYNA Users Conference*, Dearborn, MI, 2002; LSTC and Engineering Technology Associates, Inc. (ETA).

NO. OF  
COPIES ORGANIZATION

1 DEFENSE TECHNICAL  
1 DEFENSE TECHNICAL  
(PDF INFORMATION CTR  
ONLY) DTIC OCA  
8725 JOHN J KINGMAN RD  
STE 0944  
FT BELVOIR VA 22060-6218

1 COMMANDING GENERAL  
US ARMY MATERIEL CMD  
AMCRDA TF  
5001 EISENHOWER AVE  
ALEXANDRIA VA 22333-0001

1 INST FOR ADVNCD TCHNLGY  
THE UNIV OF TEXAS  
AT AUSTIN  
3925 W BRAKER LN STE 400  
AUSTIN TX 78759-5316

1 US MILITARY ACADEMY  
MATH SCI CTR EXCELLENCE  
MADN MATH  
THAYER HALL  
WEST POINT NY 10996-1786

1 DIRECTOR  
US ARMY RESEARCH LAB  
IMNE AD IM DR  
2800 POWDER MILL RD  
ADELPHI MD 20783-1197

3 DIRECTOR  
US ARMY RESEARCH LAB  
AMSRD ARL CI OK TL  
2800 POWDER MILL RD  
ADELPHI MD 20783-1197

3 DIRECTOR  
US ARMY RESEARCH LAB  
AMSRD ARL CS IS T  
2800 POWDER MILL RD  
ADELPHI MD 20783-1197

NO. OF  
COPIES ORGANIZATION

ABERDEEN PROVING GROUND

1 DIR USARL  
AMSRD ARL CI OK TP (BLDG 4600)

NO. OF  
COPIES ORGANIZATION

1 DIRECTOR  
US ARMY RESEARCH LAB  
AMSRD ARL SE L  
D SNIDER  
2800 POWDER MILL RD  
ADELPHI MD 20783-1197

1 DIRECTOR  
US ARMY RESEARCH LAB  
AMSRD ARL SE DE  
R ATKINSON  
2800 POWDER MILL RD  
ADELPHI MD 20783-1197

5 DIRECTOR  
US ARMY RESEARCH LAB  
AMSRD ARL WM MB  
A ABRAHAMIAN  
M BERMAN  
M CHOWDHURY  
T LI  
E SZYMANSKI  
2800 POWDER MILL RD  
ADELPHI MD 20783-1197

1 COMMANDER  
US ARMY MATERIEL CMD  
AMXMI INT  
5001 EISENHOWER AVE  
ALEXANDRIA VA 22333-0001

2 PM MAS  
SFAE AMO MAS MC  
PICATINNY ARSENAL NJ  
07806-5000

3 COMMANDER  
US ARMY ARDEC  
AMSTA AR CC  
M PADGETT  
J HEDDERICH  
H OPAT  
PICATINNY ARSENAL NJ  
07806-5000

2 COMMANDER  
US ARMY ARDEC  
AMSTA AR AE WW  
E BAKER  
J PEARSON  
PICATINNY ARSENAL NJ  
07806-5000

NO. OF  
COPIES ORGANIZATION

1 COMMANDER  
US ARMY ARDEC  
AMSTA AR FSE  
PICATINNY ARSENAL NJ  
07806-5000

1 COMMANDER  
US ARMY ARDEC  
AMSTA AR TD  
PICATINNY ARSENAL NJ  
07806-5000

13 COMMANDER  
US ARMY ARDEC  
AMSTA AR CCH A  
F ALTAMURA  
M NICOLICH  
M PALATHINGUL  
D VO  
R HOWELL  
A VELLA  
M YOUNG  
L MANOLE  
S MUSALLI  
R CARR  
M LUCIANO  
E LOGSDEN  
T LOUZEIRO  
PICATINNY ARSENAL NJ  
07806-5000

1 COMMANDER  
US ARMY ARDEC  
AMSTA AR CCH P  
J LUTZ  
PICATINNY ARSENAL NJ  
07806-5000

1 COMMANDER  
US ARMY ARDEC  
AMSTA AR FSF T  
C LIVECCHIA  
PICATINNY ARSENAL NJ  
07806-5000

1 COMMANDER  
US ARMY ARDEC  
AMSTA ASF  
PICATINNY ARSENAL NJ  
07806-5000

<u>NO. OF COPIES</u>	<u>ORGANIZATION</u>
1	COMMANDER US ARMY ARDEC AMSTA AR QAC T C J PAGE PICATINNY ARSENAL NJ 07806-5000
1	COMMANDER US ARMY ARDEC AMSTA AR M D DEMELLA PICATINNY ARSENAL NJ 07806-5000
3	COMMANDER US ARMY ARDEC AMSTA AR FSA A WARNASH B MACHAK M CHIEFA PICATINNY ARSENAL NJ 07806-5000
2	COMMANDER US ARMY ARDEC AMSTA AR FSP G M SCHIKSNIS D CARLUCCI PICATINNY ARSENAL NJ 07806-5000
2	COMMANDER US ARMY ARDEC AMSTA AR CCH C H CHANIN S CHICO PICATINNY ARSENAL NJ 07806-5000
1	COMMANDER US ARMY ARDEC AMSTA AR QAC T D RIGLIOSO PICATINNY ARSENAL NJ 07806-5000
1	COMMANDER US ARMY ARDEC AMSTA AR WET T SACHAR BLDG 172 PICATINNY ARSENAL NJ 07806-5000

<u>NO. OF COPIES</u>	<u>ORGANIZATION</u>
1	US ARMY ARDEC INTELLIGENCE SPECIALIST AMSTA AR WEL F M GUERRIERE PICATINNY ARSENAL NJ 07806-5000
10	COMMANDER US ARMY ARDEC AMSTA AR CCH B P DONADIA F DONLON P VALENTI C KNUTSON G EUSTICE K HENRY J MCNABOC G WAGNECZ R SAYER F CHANG PICATINNY ARSENAL NJ 07806-5000
6	COMMANDER US ARMY ARDEC AMSTA AR CCL F PUZYCKI R MCHUGH D CONWAY E JAROSZEWSKI R SCHLENNER M CLUNE PICATINNY ARSENAL NJ 07806-5000
1	PM ARMS SFAE GCSS ARMS BLDG 171 PICATINNY ARSENAL NJ 07806-5000
1	COMMANDER US ARMY ARDEC AMSTA AR WEA J BRESCIA PICATINNY ARSENAL NJ 07806-5000
1	PM MAS SFAE AMO MAS PICATINNY ARSENAL NJ 07806-5000

NO. OF  
COPIES ORGANIZATION

1 PM MAS  
SFAE AMO MAS  
CHIEF ENGINEER  
PICATINNY ARSENAL NJ  
07806-5000

1 PM MAS  
SFAE AMO MAS PS  
PICATINNY ARSENAL NJ  
07806-5000

2 PM MAS  
SFAE AMO MAS LC  
PICATINNY ARSENAL NJ  
07806-5000

1 COMMANDER  
US ARMY ARDEC  
PRODUCTION BASE  
MODERN ACTY  
AMSMC PBM K  
PICATINNY ARSENAL NJ  
07806-5000

1 COMMANDER  
US ARMY TACOM  
PM COMBAT SYSTEMS  
SFAE GCS CS  
6501 ELEVEN MILE RD  
WARREN MI 48397-5000

1 COMMANDER  
US ARMY TACOM  
AMSTA SF  
WARREN MI 48397-5000

1 DIRECTOR  
AIR FORCE RESEARCH LAB  
MLLMD  
D MIRACLE  
2230 TENTH ST  
WRIGHT PATTERSON AFB OH  
45433-7817

1 OFC OF NAVAL RESEARCH  
J CHRISTODOULOU  
ONR CODE 332  
800 N QUINCY ST  
ARLINGTON VA 22217-5600

1 US ARMY CERL  
R LAMPO  
2902 NEWMARK DR  
CHAMPAIGN IL 61822

NO. OF  
COPIES ORGANIZATION

1 COMMANDER  
US ARMY TACOM  
PM SURVIVABLE SYSTEMS  
SFAE GCSS W GSI H  
M RYZYI  
6501 ELEVEN MILE RD  
WARREN MI 48397-5000

1 COMMANDER  
US ARMY TACOM  
CHIEF ABRAMS TESTING  
SFAE GCSS W AB QT  
T KRASKIEWICZ  
6501 ELEVEN MILE RD  
WARREN MI 48397-5000

1 COMMANDER  
WATERVLIET ARSENAL  
SMCWV QAE Q  
B VANINA  
BLDG 44  
WATERVLIET NY 12189-4050

1 TNG, DOC, & CBT DEV  
ATZK TDD IRSA  
A POMEY  
FT KNOX KY 40121

2 HQ IOC TANK  
AMMUNITION TEAM  
AMSIO SMT  
R CRAWFORD  
W HARRIS  
ROCK ISLAND IL 61299-6000

2 COMMANDER  
US ARMY AMCOM  
AVIATION APPLIED TECH DIR  
J SCHUCK  
FT EUSTIS VA 23604-5577

1 NSWC  
DAHLGREN DIV CODE G06  
DAHLGREN VA 22448

2 US ARMY CORPS OF ENGR  
CERD C  
T LIU  
CEW ET  
T TAN  
20 MASSACHUSETTS AVE NW  
WASHINGTON DC 20314

NO. OF  
COPIES ORGANIZATION

1 US ARMY COLD REGIONS  
RSCH & ENGRNG LAB  
P DUTTA  
72 LYME RD  
HANOVER NH 03755

14 COMMANDER  
US ARMY TACOM  
AMSTA TR R  
R MCCLELLAND  
D THOMAS  
J BENNETT  
D HANSEN  
AMSTA JSK  
S GOODMAN  
J FLORENCE  
K IYER  
D TEMPLETON  
A SCHUMACHER  
AMSTA TR D  
D OSTBERG  
L HINOJOSA  
B RAJU  
AMSTA CS SF  
H HUTCHINSON  
F SCHWARZ  
WARREN MI 48397-5000

14 BENET LABS  
AMSTA AR CCB  
R FISCELLA  
M SOJA  
E KATHE  
M SCAVULO  
G SPENCER  
P WHEELER  
S KRUPSKI  
J VASILAKIS  
G FRIAR  
R HASENBEIN  
AMSTA CCB R  
S SOPOK  
E HYLAND  
D CRAYON  
R DILLON  
WATERVLIET NY 12189-4050

1 USA SBCCOM PM SOLDIER SPT  
AMSSB PM RSS A  
J CONNORS  
KANSAS ST  
NATICK MA 01760-5057

NO. OF  
COPIES ORGANIZATION

1 NSWC  
TECH LIBRARY CODE 323  
17320 DAHLGREN RD  
DAHLGREN VA 22448

2 USA SBCCOM  
MATERIAL SCIENCE TEAM  
AMSSB RSS  
J HERBERT  
M SENNETT  
KANSAS ST  
NATICK MA 01760-5057

2 OFC OF NAVAL RESEARCH  
D SIEGEL CODE 351  
J KELLY  
800 N QUINCY ST  
ARLINGTON VA 22217-5660

1 NSWC  
CRANE DIVISION  
M JOHNSON CODE 20H4  
LOUISVILLE KY 40214-5245

2 NSWC  
U SORATHIA  
C WILLIAMS CD 6551  
9500 MACARTHUR BLVD  
WEST BETHESDA MD 20817

2 COMMANDER  
NSWC  
CARDEROCK DIVISION  
R PETERSON CODE 2020  
M CRITCHFIELD CODE 1730  
BETHESDA MD 20084

8 DIRECTOR  
US ARMY NGIC  
D LEITER MS 404  
M HOLTUS MS 301  
M WOLFE MS 307  
S MINGLEDORF MS 504  
J GASTON MS 301  
W GSTATTENBAUER MS 304  
R WARNER MS 305  
J CRIDER MS 306  
2055 BOULDERS RD  
CHARLOTTESVILLE VA  
22911-8318

<u>NO. OF COPIES</u>	<u>ORGANIZATION</u>
1	NAVAL SEA SYSTEMS CMD D LIESE 1333 ISAAC HULL AVE SE 1100 WASHINGTON DC 20376-1100
1	EXPEDITIONARY WARFARE DIV N85 F SHOUP 2000 NAVY PENTAGON WASHINGTON DC 20350-2000
8	US ARMY SBCCOM SOLDIER SYSTEMS CENTER BALLISTICS TEAM J WARD W ZUKAS P CUNNIFF J SONG MARINE CORPS TEAM J MACKIEWICZ BUS AREA ADVOCACY TEAM W HASKELL AMSSB RCP SS W NYKVIST S BEAUDOIN KANSAS ST NATICK MA 01760-5019
7	US ARMY RESEARCH OFC A CROWSON H EVERETT J PRATER G ANDERSON D STEPP D KISEROW J CHANG PO BOX 12211 RESEARCH TRIANGLE PARK NC 27709-2211
1	AFRL MLBC 2941 P ST RM 136 WRIGHT PATTERSON AFB OH 45433-7750
1	DIRECTOR LOS ALAMOS NATL LAB F L ADDESSIO T 3 MS 5000 PO BOX 1633 LOS ALAMOS NM 87545

<u>NO. OF COPIES</u>	<u>ORGANIZATION</u>
8	NSWC J FRANCIS CODE G30 D WILSON CODE G32 R D COOPER CODE G32 J FRAYSSE CODE G33 E ROWE CODE G33 T DURAN CODE G33 L DE SIMONE CODE G33 R HUBBARD CODE G33 DAHLGREN VA 22448
1	NSWC CARDEROCK DIVISION R CRANE CODE 6553 9500 MACARTHUR BLVD WEST BETHESDA MD 20817-5700
1	AFRL MLSS R THOMSON 2179 12TH ST RM 122 WRIGHT PATTERSON AFB OH 45433-7718
2	AFRL F ABRAMS J BROWN BLDG 653 2977 P ST STE 6 WRIGHT PATTERSON AFB OH 45433-7739
5	DIRECTOR LLNL R CHRISTENSEN S DETERESA F MAGNESS M FINGER MS 313 M MURPHY L 282 PO BOX 808 LIVERMORE CA 94550
1	AFRL MLS OL L COULTER 5851 F AVE BLDG 849 RM AD1A HILL AFB UT 84056-5713
1	OSD JOINT CCD TEST FORCE OSD JCCD R WILLIAMS 3909 HALLS FERRY RD VICKSBURG MS 29180-6199

<u>NO. OF</u> <u>COPIES</u>	<u>ORGANIZATION</u>
3	DARPA M VANFOSSEN S WAX L CHRISTODOULOU 3701 N FAIRFAX DR ARLINGTON VA 22203-1714
2	SERDP PROGRAM OFC PM P2 C PELLERIN B SMITH 901 N STUART ST STE 303 ARLINGTON VA 22203
1	OAK RIDGE NATL LAB R M DAVIS PO BOX 2008 OAK RIDGE TN 37831-6195
1	OAK RIDGE NATL LAB C EBERLE MS 8048 PO BOX 2008 OAK RIDGE TN 37831
3	DIRECTOR SANDIA NATL LABS APPLIED MECHS DEPT MS 9042 J HANDROCK Y R KAN J LAUFFER PO BOX 969 LIVERMORE CA 94551-0969
1	OAK RIDGE NATL LAB C D WARREN MS 8039 PO BOX 2008 OAK RIDGE TN 37831
4	NIST M VANLANDINGHAM MS 8621 J CHIN MS 8621 J MARTIN MS 8621 D DUTHINH MS 8611 100 BUREAU DR GAITHERSBURG MD 20899
1	HYDROGEOLOGIC INC SERDP ESTCP SPT OFC S WALSH 1155 HERNDON PKWY STE 900 HERNDON VA 20170

<u>NO. OF</u> <u>COPIES</u>	<u>ORGANIZATION</u>
3	NASA LANGLEY RESEARCH CTR AMSRD ARL VS W ELBER MS 266 F BARTLETT JR MS 266 G FARLEY MS 266 HAMPTON VA 23681-0001
1	NASA LANGLEY RESEARCH CTR T GATES MS 188E HAMPTON VA 23661-3400
1	FHWA E MUNLEY 6300 GEORGETOWN PIKE MCLEAN VA 22101
1	USDOT FEDERAL RAILROAD M FATEH RDV 31 WASHINGTON DC 20590
3	CYTEC FIBERITE R DUNNE D KOHLI R MAYHEW 1300 REVOLUTION ST HAVRE DE GRACE MD 21078
1	DIRECTOR NGIC IANG TMT 2055 BOULDERS RD CHARLOTTESVILLE VA 22911-8318
1	SIOUX MFG B KRIEL PO BOX 400 FT TOTTEN ND 58335
2	3TEX CORP A BOGDANOVICH J SINGLETARY 109 MACKENAN DR CARY NC 27511
1	3M CORP J SKILDUM 3M CENTER BLDG 60 IN 01 ST PAUL MN 55144-1000

NO. OF  
COPIES ORGANIZATION

1 DIRECTOR  
DEFENSE INTLLGNC AGENCY  
TA 5  
K CRELLING  
WASHINGTON DC 20310

1 ADVANCED GLASS FIBER YARNS  
T COLLINS  
281 SPRING RUN LANE STE A  
DOWNINGTON PA 19335

1 COMPOSITE MATERIALS INC  
D SHORTT  
19105 63 AVE NE  
PO BOX 25  
ARLINGTON WA 98223

1 JPS GLASS  
L CARTER  
PO BOX 260  
SLATER RD  
SLATER SC 29683

1 COMPOSITE MATERIALS INC  
R HOLLAND  
11 JEWEL CT  
ORINDA CA 94563

1 COMPOSITE MATERIALS INC  
C RILEY  
14530 S ANSON AVE  
SANTA FE SPRINGS CA 90670

2 SIMULA  
J COLTMAN  
R HUYETT  
10016 S 51ST ST  
PHOENIX AZ 85044

2 PROTECTION MATERIALS INC  
M MILLER  
F CRILLEY  
14000 NW 58 CT  
MIAMI LAKES FL 33014

2 FOSTER MILLER  
M ROYLANCE  
W ZUKAS  
195 BEAR HILL RD  
WALTHAM MA 02354-1196

NO. OF  
COPIES ORGANIZATION

1 ROM DEVELOPMENT CORP  
R O MEARA  
136 SWINEBURNE ROW  
BRICK MARKET PLACE  
NEWPORT RI 02840

2 TEXTRON SYSTEMS  
T FOLTZ  
M TREASURE  
1449 MIDDLESEX ST  
LOWELL MA 01851

1 O GARA HESS & EISENHARDT  
M GILLESPIE  
9113 LESAINTE DR  
FAIRFIELD OH 45014

2 MILLIKEN RESEARCH CORP  
H KUHN  
M MACLEOD  
PO BOX 1926  
SPARTANBURG SC 29303

1 CONNEAUGHT INDUSTRIES INC  
J SANTOS  
PO BOX 1425  
COVENTRY RI 02816

1 ARMTEC DEFENSE PRODUCTS  
S DYER  
85 901 AVE 53  
PO BOX 848  
COACHELLA CA 92236

1 NATL COMPOSITE CTR  
T CORDELL  
2000 COMPOSITE DR  
KETTERING OH 45420

3 PACIFIC NORTHWEST LAB  
M SMITH  
G VAN ARSDALE  
R SHIPPELL  
PO BOX 999  
RICHLAND WA 99352

1 SAIC  
M PALMER  
1410 SPRING HILL RD STE 400  
MS SH4 5  
MCLEAN VA 22102

<u>NO. OF COPIES</u>	<u>ORGANIZATION</u>
1	ALLIANT TECHSYSTEMS INC 4700 NATHAN LN N PLYMOUTH MN 55442-2512
1	APPLIED COMPOSITES W GRISCH 333 NORTH SIXTH ST ST CHARLES IL 60174
1	CUSTOM ANALYTICAL ENG SYS INC A ALEXANDER 13000 TENSOR LANE NE FLINTSTONE MD 21530
1	AAI CORP DR N B MCNELLIS PO BOX 126 HUNT VALLEY MD 21030-0126
1	OFC DEPUTY UNDER SEC DEFNS J THOMPSON 1745 JEFFERSON DAVIS HWY CRYSTAL SQ 4 STE 501 ARLINGTON VA 22202
3	ALLIANT TECHSYSTEMS INC J CONDON E LYNAM J GERHARD WV01 16 STATE RT 956 PO BOX 210 ROCKET CENTER WV 26726-0210
1	PROJECTILE TECHNOLOGY INC 515 GILES ST HAVRE DE GRACE MD 21078
1	HEXCEL INC R BOE PO BOX 18748 SALT LAKE CITY UT 84118
1	PRATT & WHITNEY C WATSON 400 MAIN ST MS 114 37 EAST HARTFORD CT 06108

<u>NO. OF COPIES</u>	<u>ORGANIZATION</u>
5	NORTHROP GRUMMAN B IRWIN K EVANS D EWART A SHREKENHAMER J MCGLYNN BLDG 160 DEPT 3700 1100 WEST HOLLYVALE ST AZUSA CA 91701
1	HERCULES INC HERCULES PLAZA WILMINGTON DE 19894
1	BRIGS COMPANY J BACKOFEN 2668 PETERBOROUGH ST HERNDON VA 22071-2443
1	ZERNOW TECHNICAL SERVICES L ZERNOW 425 W BONITA AVE STE 208 SAN DIMAS CA 91773
1	GENERAL DYNAMICS OTS L WHITMORE 10101 NINTH ST NORTH ST PETERSBURG FL 33702
2	GENERAL DYNAMICS OTS FLINCHBAUGH DIV K LINDE T LYNCH PO BOX 127 RED LION PA 17356
1	GKN WESTLAND AEROSPACE D OLDS 450 MURDOCK AVE MERIDEN CT 06450-8324
2	BOEING ROTORCRAFT P MINGURT P HANDEL 800 B PUTNAM BLVD WALLINGFORD PA 19086

<u>NO. OF</u> <u>COPIES</u>	<u>ORGANIZATION</u>	<u>NO. OF</u> <u>COPIES</u>	<u>ORGANIZATION</u>
5	SIKORSKY AIRCRAFT G JACARUSO T CARSTENSAN B KAY S GARBO MS S330A J ADELMANN 6900 MAIN ST PO BOX 9729 STRATFORD CT 06497-9729	1	NORTHROP GRUMMAN CORP ELECTRONIC SENSORS & SYSTEMS DIV E SCHOCH MS V 16 1745A W NURSERY RD LINTHICUM MD 21090
1	AEROSPACE CORP G HAWKINS M4 945 2350 E EL SEGUNDO BLVD EL SEGUNDO CA 90245	1	GDLS DIVISION D BARTLE PO BOX 1901 WARREN MI 48090
2	CYTEC FIBERITE M LIN W WEB 1440 N KRAEMER BLVD ANAHEIM CA 92806	2	GDLS D REES M PASIK PO BOX 2074 WARREN MI 48090-2074
2	UDLP G THOMAS M MACLEAN PO BOX 58123 SANTA CLARA CA 95052	1	GDLS MUSKEGON OPER M SOIMAR 76 GETTY ST MUSKEGON MI 49442
1	UDLP WARREN OFC A LEE 31201 CHICAGO RD SOUTH SUITE B102 WARREN MI 48093	1	GENERAL DYNAMICS AMPHIBIOUS SYS SURVIVABILITY LEAD G WALKER 991 ANNAPOLIS WAY WOODBIDGE VA 22191
2	UDLP R BRYNSVOLD P JANKE MS 170 4800 EAST RIVER RD MINNEAPOLIS MN 55421-1498	6	INST FOR ADVANCED TECH H FAIR I MCNAB P SULLIVAN S BLESS W REINECKE C PERSAD 3925 W BRAKER LN STE 400 AUSTIN TX 78759-5316
1	LOCKHEED MARTIN SKUNK WORKS D FORTNEY 1011 LOCKHEED WAY PALMDALE CA 93599-2502	1	ARROW TECH ASSOC 1233 SHELBURNE RD STE D8 SOUTH BURLINGTON VT 05403-7700
1	LOCKHEED MARTIN R FIELDS 5537 PGA BLVD SUITE 4516 ORLANDO FL 32839	1	R EICHELBERGER CONSULTANT 409 W CATHERINE ST BEL AIR MD 21014-3613

<u>NO. OF COPIES</u>	<u>ORGANIZATION</u>
1	SAIC G CHRYSSOMALLIS 8500 NORMANDALE LAKE BLVD SUITE 1610 BLOOMINGTON MN 55437-3828
1	UCLA MANE DEPT ENGR IV H T HAHN LOS ANGELES CA 90024-1597
2	UNIV OF DAYTON RESEARCH INST R Y KIM A K ROY 300 COLLEGE PARK AVE DAYTON OH 45469-0168
1	UMASS LOWELL PLASTICS DEPT N SCHOTT 1 UNIVERSITY AVE LOWELL MA 01854
1	IIT RESEARCH CTR D ROSE 201 MILL ST ROME NY 13440-6916
1	GA TECH RESEARCH INST GA INST OF TCHNLGY P FRIEDERICH ATLANTA GA 30392
1	MICHIGAN ST UNIV MSM DEPT R AVERILL 3515 EB EAST LANSING MI 48824-1226
1	UNIV OF WYOMING D ADAMS PO BOX 3295 LARAMIE WY 82071
1	PENN STATE UNIV R S ENGEL 245 HAMMOND BLDG UNIVERSITY PARK PA 16801

<u>NO. OF COPIES</u>	<u>ORGANIZATION</u>
2	PENN STATE UNIV R MCNITT C BAKIS 212 EARTH ENGR SCIENCES BLDG UNIVERSITY PARK PA 16802
1	PURDUE UNIV SCHOOL OF AERO & ASTRO C T SUN W LAFAYETTE IN 47907-1282
1	STANFORD UNIV DEPT OF AERONAUTICS & AEROBALLISTICS S TSAI DURANT BLDG STANFORD CA 94305
1	UNIV OF MAINE ADV STR & COMP LAB R LOPEZ ANIDO 5793 AEWB BLDG ORONO ME 04469-5793
1	JOHNS HOPKINS UNIV APPLIED PHYSICS LAB P WIENHOLD 11100 JOHNS HOPKINS RD LAUREL MD 20723-6099
1	UNIV OF DAYTON J M WHITNEY COLLEGE PARK AVE DAYTON OH 45469-0240
1	NORTH CAROLINA ST UNIV CIVIL ENGINEERING DEPT W RASDORF PO BOX 7908 RALEIGH NC 27696-7908
5	UNIV OF DELAWARE CTR FOR COMPOSITE MTRLS J GILLESPIE M SANTARE S YARLAGADDA S ADVANI D HEIDER 201 SPENCER LAB NEWARK DE 19716

<u>NO. OF COPIES</u>	<u>ORGANIZATION</u>
1	DEPT OF MTRLS SCIENCE & ENGRG UNIV OF ILLINOIS AT URBANA CHAMPAIGN J ECONOMY 1304 WEST GREEN ST 115B URBANA IL 61801
1	UNIV OF MARYLAND DEPT OF AEROSPACE ENGRG A J VIZZINI COLLEGE PARK MD 20742
1	DREXEL UNIV A S D WANG 3141 CHESTNUT ST PHILADELPHIA PA 19104
3	UNIV OF TEXAS AT AUSTIN CTR FOR ELECTROMECHANICS J PRICE A WALLS J KITZMILLER 10100 BURNET RD AUSTIN TX 78758-4497
3	VA POLYTECHNICAL INST & STATE UNIV DEPT OF ESM M W HYER K REIFSNIDER R JONES BLACKSBURG VA 24061-0219
1	SOUTHWEST RESEARCH INST ENGR & MATL SCIENCES DIV J RIEGEL 6220 CULEBRA RD PO DRAWER 28510 SAN ANTONIO TX 78228-0510
1	BATELLE NATICK OPERS B HALPIN 313 SPEEN ST NATICK MA 01760
3	DIRECTOR US ARMY RESEARCH LAB AMSRD ARL WM MB A FRYDMAN 2800 POWDER MILL RD ADELPHI MD 20783-1197

<u>NO. OF COPIES</u>	<u>ORGANIZATION</u>
	<u>ABERDEEN PROVING GROUND</u>
1	US ARMY ATC CSTE DTC AT AC I W C FRAZER 400 COLLERAN RD APG MD 21005-5059
91	DIR USARL AMSRD ARL CI AMSRD ARL O AP EG M ADAMSON AMSRD ARL SL BA AMSRD ARL SL BB D BELY AMSRD ARL WM J SMITH H WALLACE AMSRD ARL WM B A HORST T KOGLER AMSRD ARL WM BA D LYON AMSRD ARL WM BC J NEWILL P PLOSTINS A ZIELINSKI AMSRD ARL WM BD P CONROY B FORCH M LEADORE C LEVERITT R LIEB R PESCE RODRIGUEZ B RICE AMSRD ARL WM BF S WILKERSON AMSRD ARL WM M B FINK J MCCAULEY AMSRD ARL WM MA L GHIORSE S MCKNIGHT E WETZEL AMSRD ARL WM MB J BENDER T BOGETTI L BURTON R CARTER K CHO W DE ROSSET G DEWING R DOWDING W DRYSDALE

NO. OF  
COPIES ORGANIZATION

R EMERSON  
D HENRY  
D HOPKINS  
R KASTE  
L KECSKES  
M MINNICINO  
B POWERS  
D SNOHA  
J SOUTH  
M STAKER  
J SWAB  
J TZENG  
AMSRD ARL WM MC  
J BEATTY  
R BOSSOLI  
E CHIN  
S CORNELISON  
D GRANVILLE  
B HART  
J LASALVIA  
J MONTGOMERY  
F PIERCE  
E RIGAS  
W SPURGEON  
AMSRD ARL WM MD  
B CHEESEMAN  
P DEHMER  
R DOOLEY  
G GAZONAS  
S GHORSE  
C HOPPEL  
M KLUSEWITZ  
W ROY  
J SANDS  
D SPAGNUOLO  
S WALSH  
S WOLF  
AMSRD ARL WM RP  
J BORNSTEIN  
C SHOEMAKER  
AMSRD ARL WM T  
B BURNS  
AMSRD ARL WM TA  
W BRUCHEY  
M BURKINS  
W GILLICH  
B GOOCH  
T HAVEL  
E HORWATH  
M NORMANDIA  
J RUNYEON  
M ZOLTOSKI

NO. OF  
COPIES ORGANIZATION

AMSRD ARL WM TB  
P BAKER  
AMSRD ARL WM TC  
R COATES  
AMSRD ARL WM TD  
D DANDEKAR  
T HADUCH  
T MOYNIHAN  
M RAFTENBERG  
S SCHOENFELD  
T WEERASOORIYA  
AMSRD ARL WM TE  
A NILER  
J POWELL

NO. OF  
COPIES ORGANIZATION

1 LTD  
R MARTIN  
MERL  
TAMWORTH RD  
HERTFORD SG13 7DG  
UK

1 SMC SCOTLAND  
P W LAY  
DERA ROSYTH  
ROSYTH ROYAL DOCKYARD  
DUNFERMLINE FIFE KY 11 2XR  
UK

1 CIVIL AVIATION  
ADMINSTRATION  
T GOTTESMAN  
PO BOX 8  
BEN GURION INTRNL AIRPORT  
LOD 70150  
ISRAEL

1 AEROSPATIALE  
S ANDRE  
A BTE CC RTE MD132  
316 ROUTE DE BAYONNE  
TOULOUSE 31060  
FRANCE

1 DRA FORT HALSTEAD  
P N JONES  
SEVEN OAKS KENT TN 147BP  
UK

1 SWISS FEDERAL ARMAMENTS  
WKS  
W LANZ  
ALLMENDSTRASSE 86  
3602 THUN  
SWITZERLAND

1 DYNAMEC RESEARCH LAB  
AKE PERSSON  
BOX 201  
SE 151 23 SODERTALJE  
SWEDEN

NO. OF  
COPIES ORGANIZATION

1 ISRAEL INST OF TECHLGY  
S BODNER  
FACULTY OF MECHANICAL  
ENGR  
HAIFA 3200  
ISRAEL

1 DSTO  
WEAPONS SYSTEMS DIVISION  
N BURMAN RLLWS  
SALISBURY  
SOUTH AUSTRALIA 5108  
AUSTRALIA

1 DEF RES ESTABLISHMENT  
VALCARTIER  
A DUPUIS  
2459 BLVD PIE XI NORTH  
VALCARTIER QUEBEC  
CANADA  
PO BOX 8800 COURCELETTE  
GOA IRO QUEBEC  
CANADA

1 ECOLE POLYTECH  
J MANSON  
DMX LTC  
CH 1015 LAUSANNE  
SWITZERLAND

1 TNO DEFENSE RESEARCH  
R IJSSELSTEIN  
ACCOUNT DIRECTOR  
R&D ARMEE  
PO BOX 6006  
2600 JA DELFT  
THE NETHERLANDS

2 FOA NATL DEFENSE RESEARCH  
ESTAB  
DIR DEPT OF WEAPONS &  
PROTECTION  
B JANZON  
R HOLMLIN  
S 172 90 STOCKHOLM  
SWEDEN

NO. OF  
COPIES ORGANIZATION

- 2 DEFENSE TECH & PROC  
AGENCY GROUND  
I CREWTHER  
GENERAL HERZOG HAUS  
3602 THUN  
SWITZERLAND
  
- 1 MINISTRY OF DEFENCE  
RAFAEL  
ARMAMENT DEVELOPMENT  
AUTH  
M MAYSELESS  
PO BOX 2250  
HAIFA 31021  
ISRAEL
  
- 1 TNO DEFENSE RESEARCH  
I H PASMAN  
POSTBUS 6006  
2600 JA DELFT  
THE NETHERLANDS
  
- 1 B HIRSCH  
TACHKEMONY ST 6  
NETAMUA 42611  
ISRAEL
  
- 1 DEUTSCHE AEROSPACE AG  
DYNAMICS SYSTEMS  
M HELD  
PO BOX 1340  
D 86523 SCHROBENHAUSEN  
GERMANY

INTENTIONALLY LEFT BLANK.